https://doi.org/10.5194/egusphere-2026-4268
Preprint. Discussion started: 5 August 2026

Magnitude and controls of snow sublimation at a high-elevation Swiss Alpine site

Isabella Anglin[1], Adriaan J. Teuling[2], Marius G. Floriancic[3], Michael Lehning[1,4], and Harsh Beria[1,3]

[1]WSL Institute for Snow and Avalanche Research SLF, Davos, Switzerland
[2]Hydrology and Environmental Hydraulics (HWM) Group, Wageningen University, Wageningen, the Netherlands
[3]Department of Civil, Environmental and Geomatic Engineering, ETH Zurich, Zurich, Switzerland
[4]Laboratory of Cryospheric Sciences, Ecole polytechnique federale de Lausanne (EPFL), Sion, Switzerland

Correspondence: Harsh Beria (hberia@ethz.ch)

Abstract.

Surface snow sublimation remains poorly quantified in the European Alps, with previous modeling studies estimating a broad range of winter surface sublimation losses (10 to 180 mm w.e.). This creates large uncertainties in the partitioning of snow ablation between sublimation and snowmelt, with significant implications for downstream water availability, as surface mass losses through sublimation directly reduce spring meltwater availability. Field observations used to quantify surface snow sublimation throughout a winter season remain scarce due to the logistical challenges posed by high-elevation Alpine environments. To address this, we estimated surface snow sublimation using the eddy-covariance method over one full winter season (November 2024 to June 2025) at the Weissfluhjoch research site (2536 m a.s.l) in the Eastern Swiss Alps by measuring water vapor fluxes with an integrated open-path gas analyzer and sonic anemometer (IRGASON). Partial correlation analyses and explainable machine learning (XGBoost model with Shapley Additive Explanations) were used to quantify the relative importance of different meteorological variables on modeled sublimation. Over the 2024-25 winter season, cumulative net surface sublimation was 24.7 ± 18.3 mm, equivalent to 5.7 ± 4.2 % of maximum snow water equivalent, with an average daily sublimation rate of 0.15 mm d^{-1}. Nearly half of cumulative surface sublimation occurred after peak snow height was reached, between March 31, 2025 and June 1, 2025. Vapor pressure gradient and wind speed emerged as the dominant controls on surface sublimation across both statistical and machine learning approaches, while net shortwave radiation became increasingly important following peak snow height. In contrast, air temperature and snow surface temperature showed little independent predictive power once covariance with other variables was accounted for. Our findings highlight the importance of continuous eddy-covariance measurements for quantifying snow sublimation and provide one of the first winter-season estimates of surface snow sublimation in the European Alps.

1 Introduction

Snow is an essential component of the Earth's hydrological cycle. The water stored in mountain snowpacks acts as a crucial reservoir, releasing meltwater during spring thereby sustaining downstream ecosystems and livelihoods (Huss et al., 2017; Rodell et al., 2018). More than one-sixth of the world's population relies on meltwater from glaciers and seasonal snowpacks,

https://doi.org/10.5194/egusphere-2026-4268
Preprint. Discussion started: 5 August 2026

with most of this water originating in mountains (Barnett et al., 2005). In Europe, snowmelt from the Alps helps to sustain the water demands in some of Europe's largest river basins including the Rhine, Po, Danube, and Rhone, making the Alps a crucial 'water tower' (Immerzeel et al., 2019). In fact, it is estimated that over 10% of Europe's water reserves are stored in the Swiss Alps (Poussin et al., 2025).

However, not all accumulated snow contributes to downstream water availability. Snow sublimation represents a pathway through which snow is lost directly to the atmosphere, and can therefore reduce downstream water availability through snowmelt (Lundquist et al., 2024). During snow sublimation, hereafter simply referred to as sublimation, snow grains undergo a direct phase change from solid snow to water vapor, driven primarily by the difference between vapor pressure at the snow surface and vapor pressure in the ambient atmosphere (Fierz et al., 2009). Sublimation is commonly categorized into (i) surface sublimation from snowpack on the ground, (ii) canopy sublimation from snow intercepted by vegetation, and (iii) blowing snow sublimation from suspended or saltating snow particles (Mott et al., 2018; Sigmund et al., 2025). The total sublimation at a site depends on the sum of these processes (Mott et al., 2018).

Sublimation exhibits large spatial and temporal variability across environments. Previous global compilations have shown a wide range of sublimation fluxes (0.01 –2 mm d^{-1}) from surface, canopy and blowing snow sublimation, with the highest rates reported in wind-exposed high-altitude sites (0.9–2.0 mm d^{-1}) and in forests (0.4–1.2 mm d^{-1}) (Jackson and Prowse, 2009; Svoma, 2016). Most of these studies were conducted at sites in North America, with few studies carried out in the eastern Tibetan plateau, Qilian mountains, eastern Siberia, Japan and Finland. More recent studies have shown that surface sublimation can account for 16–42% of winter snowfall over Himalayan glaciers (1–3.7 mm d^{-1}) (Mandal et al., 2022; Stigter et al., 2018), 8–17% of maximum snow accumulation (0.26–0.38 mm d^{-1}) in the Colorado Rocky Mountains (Sexstone et al., 2016; Schwat et al., 2025), and 4–41% of maximum snow accumulation (0.15–0.52 mm d^{-1}) in the Owyhee Mountains in the USA (Reba et al., 2012).

Estimates of surface sublimation based on field measurements remain scarce in the European Alps, particularly at the temporal resolution required to resolve the atmospheric processes controlling snow-atmosphere vapor exchange. This limits regional estimates of sublimation losses and process-based understanding of how meteorological conditions regulate the partitioning of snow ablation between sublimation and melt. Previous modeling efforts in the Berchtesgarten National Park in Germany and in the Eastern Swiss Alps have suggested a wide range of winter surface sublimation fluxes, locally ranging from 10 to 180 mm w.e., with the highest modeled sublimation rates at mountain crests (Groot Zwaaftink et al., 2013; Strasser et al., 2008). However, to our knowledge, no study has yet quantified surface snow sublimation over a full winter season in the European Alps using high resolution eddy-covariance measurements. Such measurements are required to constrain seasonal sublimation losses and to identify the atmospheric controls that govern their temporal variability.

Surface sublimation is typically estimated using one of the following approaches: eddy-covariance method (EC), Bowen-ratio-based energy balance approach, bulk aerodynamic flux method, aerodynamic profile method and gravimetric method. Among these approaches, EC is considered the most reliable method to estimate surface sublimation (Sexstone et al., 2016), requiring high frequency (10 or 20 Hz) measurements of water vapor fluxes and vertical wind speeds. To ensure the quality of EC-derived fluxes, rigorous post-processing is required (Reba et al., 2009). The applicability of the EC method has traditionally

https://doi.org/10.5194/egusphere-2026-4268
Preprint. Discussion started: 5 August 2026

been limited in complex alpine terrain because of high instrumentation costs, limited accessibility during harsh winter conditions, and high power requirements for continuous measurements (Sexstone et al., 2016). Recently, however, a few studies have used EC flux towers in complex terrain to measure surface sublimation during shorter campaigns (Stigter et al., 2018), and through an entire winter season or even over multiple years (Reba et al., 2012; Sexstone et al., 2016; Schwat et al., 2025).

While these studies have provided new insights into sublimation dynamics in mountain landscapes, comparable investigations remain scarce in the European Alps, where the dominant controls on snow sublimation are still poorly constrained. A long list of meteorological variables has been identified as potential controls on sublimation, including vapor pressure gradient, atmosphere vapor pressure deficit, wind speed, air temperature, snow surface temperature, temperature gradients between the snow surface and the ambient atmosphere, relative humidity, net radiation, and cloud cover (Mandal et al., 2022; Sexstone et al., 2016; Reba et al., 2012; Schwat et al., 2025; Stigter et al., 2018; Svoma, 2016; Stockert et al., 2025; Beria et al., 2018). Among these variables, vapor pressure gradient, wind speed, relative humidity, and air temperature were most frequently identified as primary drivers of sublimation (Stockert et al., 2025; Sexstone et al., 2018; Reba et al., 2012). However, these variables are strongly correlated, particularly in complex mountain environments (Mandal et al., 2022). Most previous studies have relied on bivariate correlations or multiple linear regression approaches, while not explicitly accounting for correlations between variables. As a result, it remains unclear whether reported relationships reflect independent controls or covary with another more dominant driver.

In this study, we estimate surface snow sublimation using the eddy-covariance technique at a high-elevation alpine site (2536 m a.s.l) in the Eastern Swiss Alps during the winter season 2024–25. To this end, we (1) quantify the magnitude and temporal variability of surface sublimation over a full winter season, and (2) identify the dominant meteorological controls on surface sublimation using partial correlation analysis and explainable machine learning based on gradient-boosted decision trees (XGBoost) with Shapley Additive Explanations (SHAP). Through this integrated framework, this study provides novel insights into the magnitude and meteorological controls on surface snow sublimation in the Swiss Alps. Hereafter, the term sublimation refers to surface snow sublimation unless stated otherwise.

2 Study site

The Weissfluhjoch research site (46°49’47”N 9°48’33”E; WFJ) is an alpine site located in the southeastern Swiss Alps above Davos Dorf at an elevation of 2536 m a.s.l (Marty and Meister, 2012). It is situated below the Weissfluhjoch, a saddle between the upper Schanfigg and the southern Prättigau. The terrain is approximately flat and is largely sheltered by mountain ridges rising about 100 m, providing wind protection (Figure 1b). Toward the southeast, a small hill rises roughly 10 m above the site.

Since the first snow laboratory was set up in 1936 by the WSL Institute for Snow and Avalanche Research (SLF), daily weather and snow measurements have been carried out. Based on these long-term measurements, the average first date for snow cover is 18 October and the average date of snow cover disappearance is 8 July. The average annual precipitation is 1200 mm of which roughly 75% fall as snow (Marty, 2025). Winds from the northwest bring most precipitation, while winds from

https://doi.org/10.5194/egusphere-2026-4268
Preprint. Discussion started: 5 August 2026

the south drive dry and warm Föhn periods. The site experiences a climate affected by wet, maritime northern conditions and dry, continental alpine conditions (Meister, 2009).

2.1 Instrumentation

An integrated open-path gas analyzer and 3D sonic anemometer (IRGASON; Campbell Scientific) was installed at the WFJ research site in March 2024 on a mast 5.4 m above bare ground (Figure 1e). This instrument measures the water vapor concentration, air temperature and three-directional wind speed continuously at 20 Hz temporal frequency, with the raw data recorded on a CR1000 data logger (Campbell-Scientific). In addition to these high frequency measurements, other meteorological and snow variables are measured continuously at the WFJ research site at a lower temporal resolution. A summary of the main atmospheric variables, their measurement frequency and instrument uncertainty is shown in Table 1.

Table 1. Overview of snow and meteorological measurements at the Weissfluhjoch research site. Manual measurements of snow stratigraphy are taken at the research site biweekly (every two weeks) by SLF.

Measured variable	Model and manufacturer	Measurement frequency	Height above bare ground (m)	Instrument uncertainty
Air temperature	THYGAN (Meteolabor AG)	10 min	5.4	± 0.2 °C
Relative humidity	THYGAN (Meteolabor AG)	10 min	5.4	± 0.1%
Wind speed	Wind Monitor 05103 (RM Young)	10 min	6	± 1%
Wind direction	Wind Monitor 05103 (RM Young)	10 min	6	± 3°
Incoming and outgoing shortwave radiation	CM 21 pyranometer (Kipp & Zonen)	2 min	5	± 2%
Incoming and outgoing longwave radiation	Precision Infrared Radiometer (Eppley)	2 min	5	± 5 W m^{-2}
Snow depth	SR50A (Campbell Scientific)	10 min	5	± 1 cm
Snow surface temperature	Apogee SI-111 (Campbell Scientific)	10 min	5	± 0.5 °C
Snow water equivalent	SSG1000 snow scale (Sommer Messtechnik)	10 min	0	±10%
Snow stratigraphy and bulk snowpack density	Manual measurement	Biweekly		
Water vapor concentration	IRGASON (Campbell Scientific)	20 Hz	5.4	± 0.004 g m^{-3}
Vertical and horizontal wind speed and direction	IRGASON (Campbell Scientific)	20 Hz	5.4	± 1 mm s^{-1}
Sonic temperature	IRGASON (Campbell Scientific)	20 Hz	5.4	± 0.025 °C
Soil heat flux	HPF01 (HUKX)	10 min	0	± 3%

2.2 Study period

For accurately estimating snow sublimation, we only considered periods with continuous snow cover, during which soil evaporation and transpiration can be neglected, and the latent heat fluxes can be attributed to sublimation. We therefore defined winter as the period during which snow height was above 15 cm and the 5-day moving average of air temperature remained below 5°C. The snow height was conservatively chosen to ensure that no exposed rocks or bare soil was present in the footprint of the flux tower. The moving average for air temperature was selected to exclude the influence of transpiration from plants or grasses from within the footprint of the flux tower (Körner et al., 2023). The resulting snow cover period at the WFJ research

https://doi.org/10.5194/egusphere-2026-4268
Preprint. Discussion started: 5 August 2026

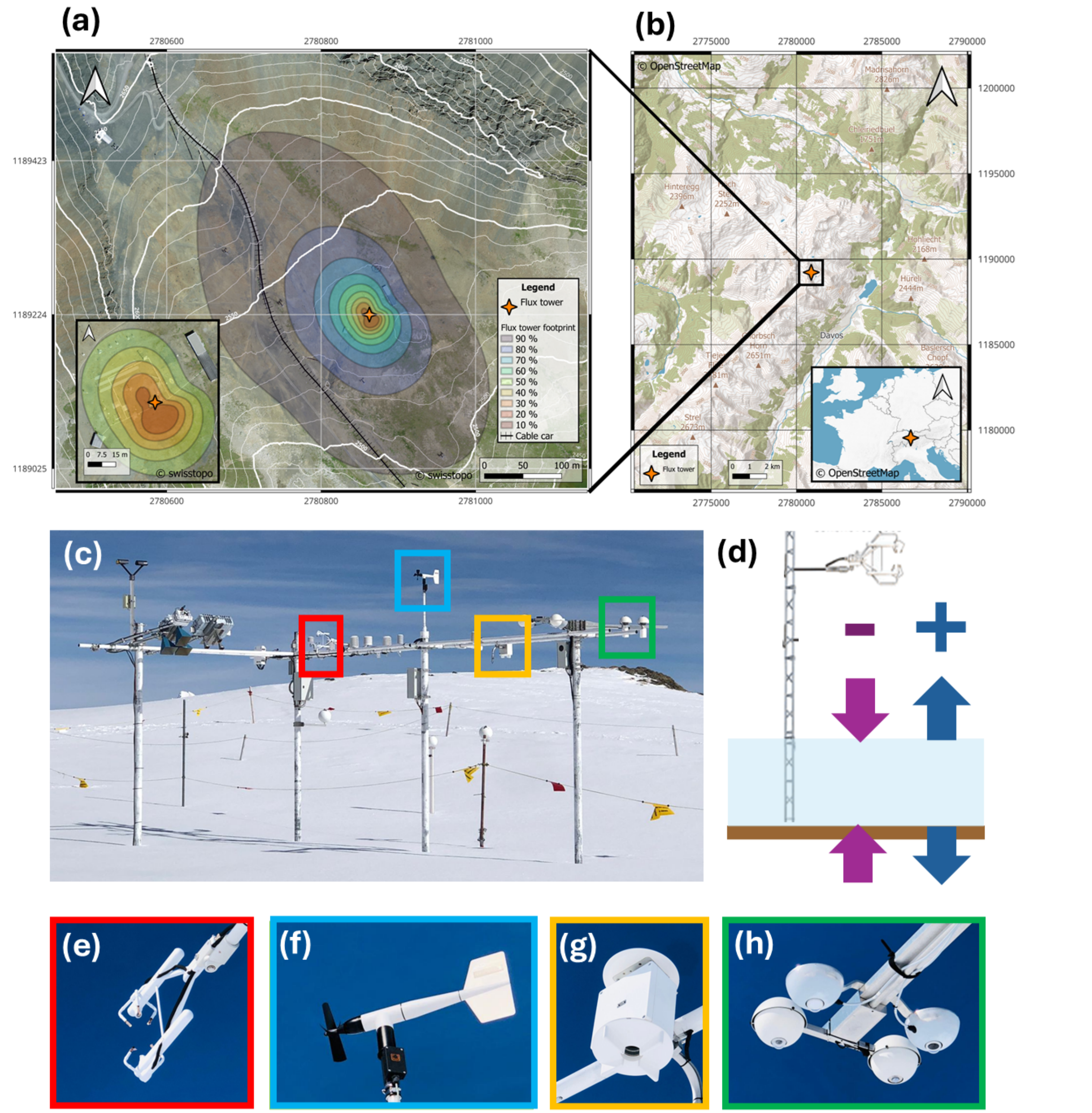

Figure 1. Overview and instrumentation of the Weissfluhjoch (WFJ) research site. (a) Close-up topographic view of the flux tower (star), including the flux footprint extent with 10 to 90% footprint contours. The footprints were calculated using the Flux Footprint Prediction model based on flux measurements during the study period (November 19, 2024 to June 1, 2025) (Kljun et al., 2015). Map source: © swisstopo. (b) Location of WFJ in Europe and in the surroundings of Davos, Switzerland. Map source: © OpenStreetMaps. (c) Measurement setup at WFJ (adapted from Lackner et al. (2022)). (d) Schematic of flux sign convention used in this paper for energy balance terms, fluxes entering the snowpack are negative, and fluxes leaving the snowpack are positive. (e) Sonic anemometer and gas analyzer (IRGASON; Campbell Scientific), (f) anemometer (05103; RM Young) (g) hygrometer (THYGAN; Meteolabor AG), (h) pyranometer (CM21; Kipp & Zonen) and precision infrared radiometer (Eppley).

https://doi.org/10.5194/egusphere-2026-4268
Preprint. Discussion started: 5 August 2026

site was from 19 November 2024 to 1 June 2025 (see Figure A1). After the cutoff date of June 1, a rapid increase in water vapor fluxes was seen, presumably reflecting the effects of soil evaporation and transpiration (Figure A1c).

3 Methods

3.1 Meteorological measurements

An overview of the meteorological measurements collected at the WFJ research site is presented in Table 1. Data gaps were addressed using variable-specific approaches. For air temperature, relative humidity, wind speed, snow depth, and soil heat flux, missing values were filled using linear interpolation. In the case of wind direction, gaps were filled using the previous valid observation. Although radiative measurements did not exhibit gaps, incoming shortwave radiation measurements were affected by a daily shadow around noon caused by the pole installed for diffuse radiation measurements. As this shadow was caused by the measurement setup and not representative of the incoming shortwave radiation at the site, the affected time steps were removed and the corresponding incoming shortwave radiation values were estimated using reflected shortwave radiation at the same time step and the albedo from the preceding time step (before noon) or the subsequent time step (after noon). Snow surface temperature measurements did not contain gaps; however, instrument heating occasionally produced values exceeding 0°C, which were subsequently capped at 0°C.

3.2 Eddy-covariance turbulent flux calculations

The sensible heat flux, Q_H, and water vapor flux, F_{H_2O}, were estimated according to the eddy covariance method as follows:

$$Q_H = \rho c_p \overline{w'T'} \tag{1}$$

and

$$F_{H_2O} = \overline{w' d'_{H_2O}} \tag{2}$$

where ρ is the air density, c_p is the specific heat of air at constant pressure, T is the sonic air temperature, w is the vertical wind speed, and d_{H_2O} is the molar density of water (LI-COR, 2025). Overbars denote the mean value, taken over the Reynolds averaging length, and primes denote deviations from the mean.

An appropriate Reynolds averaging length, τ, for water vapor fluxes was determined using both the multi-resolution flux decomposition method (MRD) (Howell and Mahrt, 1997; Vickers and Mahrt, 2003) and stationarity statistics from the steady state test by Foken and Wichura (1996). The $\overline{w' d'_{H_2O}}$ cospectrum over daytime hours (10:00–17:00) for each day throughout the winter period was calculated using MRD as implemented in the PEDDY package (Leibersperger et al., 2026). Each cospectrum was classified as stable or unstable using the mean sensible heat flux ($\overline{w'T'}$) between 10:00–17:00 (Schwat et al., 2025). A composite cospectrum for each stability class was calculated by taking the median of each τ bin (Schwat et al., 2025), and the

https://doi.org/10.5194/egusphere-2026-4268
Preprint. Discussion started: 5 August 2026

spectral gap identified according to Vickers and Mahrt (2003). Combined with results from the steady state test (Reba et al., 2009), we identified 15 minutes as a suitable time averaging length, which is in a similar range to studies in other mountainous, snow-covered terrains (Reba et al., 2009; Sexstone et al., 2016), but much shorter than the 30 minutes typically used for vegetated surfaces.

Raw high frequency data (20 Hz) from the IRGASON was corrected and processed using the LI-COR EddyPro 7 software. To improve flux calculations, dynamic metadata was provided for each timestep to account for the changing instrument height relative to snow depth, as the instruments were located at a fixed height above the surface, but snow depth changed over time. Meteorological data for incoming longwave radiation, incoming shortwave radiation, ambient pressure, relative humidity, and ambient air temperature was also provided to EddyPro 7. A 15-minute averaging length and maximum of 25% missing sample allowance was selected (Schwat et al., 2025), with all statistical screening tests to flag the raw data (Vickers and Mahrt, 1997), double-rotation for axis-tilt correction (Wilczak et al., 2001) and block averaging for de-trending. Spectral corrections were applied in both the low-frequency (Moncrieff et al., 1996) and high-frequency ranges (Fratini et al., 2012) and the covariance between water vapor and vertical wind speed was corrected for air density (Webb et al., 1980). The flagging scheme of Mauder and Foken (2004) was used to test for stationarity and fully-developed turbulence.

The latent heat flux, Q_{LE}, was calculated based on the corrected water vapor flux output, F_{H_2O}, from EddyPro 7 as follows:

$$Q_{LE} = 10^{-3} \cdot M_{H_2O} \cdot \lambda \cdot F_{H_2O} \tag{3}$$

where M_{H_2O} is the molar mass of water and λ the specific latent heat, determined by whether evaporation or sublimation occurs based on the snow surface temperature T_s:

$$\lambda = \begin{cases} \lambda_{\text{vap}} = 3{,}147{,}500 - 2{,}370 \cdot T_s & T_s \geq 273.15\ \text{K} \\ \lambda_{\text{sub}} = 2{,}874{,}694 - 149 \cdot T_s & T_s < 273.15\ \text{K} \end{cases} \tag{4}$$

Further post-processing was done with the DIIVE python toolbox according to Swiss Fluxnet standards (Hörtnagl, 2026). The quality flags of Mauder and Foken (2004) were expanded and a storage correction was applied (Montagnani et al., 2018). An overall quality control flag was determined for each timestep (Hörtnagl, 2025), with data flag of '0' and '1' retained as the fluxes prior to gap filling, and data flagged as '2' being discarded. Finally, gap-filling was performed using a random forest approach as implemented in the DIIVE software (Hörtnagl, 2026).

3.3 Surface Energy balance

The energy balance of the snowpack can be expressed as follows:

$$dUdt^{-1} = Q_* + Q_{LE} + Q_H + Q_G + Q_A \tag{5}$$

where $dUdt^{-1}$ is the net rate of energy change of internal energy in the snowpack, Q_* is the net radiation consisting of the net shortwave and net longwave radiation, Q_G is the ground heat flux at the snow-ground interface, and Q_A is the advected heat

https://doi.org/10.5194/egusphere-2026-4268
Preprint. Discussion started: 5 August 2026

flux (Sexstone et al., 2016; Lackner et al., 2022). Fluxes entering the snowpack are given a negative sign, and fluxes exiting the snowpack are given a positive sign, as seen schematically in Figure 1d. To quantify $dUdt^{-1}$ continuously throughout the winter period, detailed measurements of snow density and temperature at different layers within the snowpack, as well as the liquid water content in the snowpack, are required (Sexstone et al., 2016). Given that these measurements were not available at the WFJ research site, we chose to introduce a residual term, Q_{res} ($\mathrm{W\,m^{-2}}$), which accounted for the internal energy change and the advected energy:

$$Q_{res} = dUdt^{-1} - Q_A = Q_* + Q_{LE} + Q_H + Q_G \tag{6}$$

Our analysis therefore cannot quantify the energy balance closure at WFJ, but rather estimates the magnitude of each measured component and the residual term of Equation 6 throughout the winter period.

3.4 Quantifying sublimation

Cumulative net sublimation, M_{sub}, was calculated using the final gap-filled water vapor flux, F_{H_2O}, as follows:

$$M_{sub} = \frac{M_{H_2O}}{10^3} \int_{t_1}^{t_2} F_{H_2O} dt \tag{7}$$

in which M_{H_2O} is the molar mass of water , and t_1 and t_2 are the start and end of the winter season. The total uncertainty of the seasonal sublimation estimates was calculated through propagation of systematic uncertainties, whereby the systematic uncertainty associated with each timestep was summed (Moncrieff et al., 1996). Uncertainties in turbulent latent and sensible heat fluxes have been previously estimated to be between ±10% (Knowles et al., 2015) to ±20% (Andreas et al., 2010). We therefore conservatively estimated the systematic uncertainty for water vapor fluxes, prior to gap-filling, to be ±20%, consistent with Sexstone et al. (2016). For gap-filled timesteps, the uncertainty was quantified using the root mean square error (RMSE) of the random forest model. Random uncertainties were not considered in the seasonal estimate as they diminish with the increasing size of the dataset and have been shown to cancel out over longer timescales (Sexstone et al., 2016; Knowles et al., 2015).

3.5 Statistical drivers of sublimation

To examine the statistical relationships between meteorological variables and the estimated surface sublimation fluxes, and to assess how these relationships vary over the winter season, we used two distinct approaches: the classical partial correlation analysis and a nonlinear machine learning model.

3.5.1 Correlations and partial correlations

Pearson correlation coefficients were calculated between meteorological variables and hourly net sublimation rates for the prior to and following peak snow height, and for the full winter period. The analyzed meteorological variables included air

https://doi.org/10.5194/egusphere-2026-4268
Preprint. Discussion started: 5 August 2026

temperature, snow surface temperature, relative humidity, vapor pressure gradient (defined as the difference between saturated vapor pressure at the snow surface and actual vapor pressure at 5.4 m above ground), net radiation, net shortwave radiation, net longwave radiation, and wind speed. These variables were selected based on the physical controls on sublimation identified in previous studies (Mandal et al., 2022; Stigter et al., 2018; Sexstone et al., 2016; Reba et al., 2009). While the dependence of turbulent fluxes on environmental variables measured close to the surface is formalized in the Monin-Obukhov (MO) similarity theory as a basis of bulk flux parameterizations, it still remains interesting to quantify for specific settings the independent influence of the forcing variables and include explicitly variables not part of the MO theory such as radiation.

Because meteorological variables are often strongly correlated with each other, partial correlation coefficients were calculated to isolate the effect of individual meteorological variables, while controlling for the influence of one to three additional variables, following the methodology of Wang et al. (2022). This approach provided a conservative estimate of the independent linear association between individual predictors and surface sublimation estimates.

3.5.2 Explainable machine learning

To capture potentially nonlinear and interacting relationships between meteorological variables and sublimation, we used the eXtreme Gradient Boosting (XGBoost) algorithm to simulate sublimation rates from meteorological predictors. XGBoost is a tree-based ensemble learning method that constructs a sequence of decision trees in a boosting framework, where each successive tree reduces the residual errors of the previous ensemble, while regularization controls model complexity and limits overfitting (Chen and Guestrin, 2016). This makes it well suited for representing complex, non-linear relationships and interactions among predictors.

In this study, the target variable for the XGBoost analysis was sublimation rate, derived from non-gap-filled water vapor fluxes at 15-minute temporal resolution throughout the winter period. Predictor combinations were selected based on four groups of meteorological drivers: (i) vapor pressure gradient (representing atmospheric dryness), (ii) wind speed (representing turbulent dynamics), (iii) net shortwave radiation or net radiation (representing available surface energy), and (iv) air temperature or snow surface temperature (representing energy state close to the snowpack boundary). Each model configuration included two to four predictors, with only up to one variable selected from each group to avoid redundancy among physically similar processes. In total, 21 distinct predictor combinations were evaluated.

The dataset was split into training (80%) and testing (20%) subsets. Because the XGBoost model was used as an interpretive tool, rather than for forecasting, the train-test split was used to assess the general predictive skill. Hyperparameters were optimized separately for each predictor combination using GridSearchCV with three-fold cross-validation on the training data. The tuning procedure explored number of trees (n_estimators), maximum tree depth (max_depth), learning rate (learning_rate), and subsampling ratio (subsample). All other hyperparameters were kept at default values. Model performance was optimized using negative mean squared error (Wang et al., 2022). Final model performance was evaluated on the independent test set using the coefficient of determination (R^2) and mean squared error (MSE).

To interpret XGBoost model predictions and quantify the contribution of each predictor, we applied the SHAP framework using the TreeExplainer algorithm (Lundberg et al., 2020). SHAP decomposes each model prediction into additive contribu-

https://doi.org/10.5194/egusphere-2026-4268
Preprint. Discussion started: 5 August 2026

tions from individual input variables based on Shapley values from cooperative game theory. For each time step, the predicted sublimation rate is expressed as the sum of a baseline expectation and the individual contributions of each predictor (SHAP values).

In this study, the importance of each predictor was assessed using the mean absolute SHAP value for each predictor, calculated separately for the full winter period, as well as prior to and following peak snow height. To further examine the functional relationships between the predictors and sublimation rates, SHAP dependence plots were generated for each predictor. These plots relate predictor values to their corresponding SHAP values, thereby revealing their non-linear relationships and sensitivity patterns across the observed range of atmospheric conditions. Finally, SHAP interaction values were computed to separate main effects from interaction effects, allowing the direct effect of each predictor on surface sublimation to be distinguished from its combined influence with other meteorological variables.

4 Results

4.1 Snowpack and meteorological conditions

The 2024–25 winter period at the WFJ research site lasted from 19 November 2024 to 1 June 2025, with a peak snow height of 1.43 m recorded on 31 March 2025, indicated by the vertical gray line in Figure 2. Based on the temporal evolution of snow height, we distinguish two periods during the winter: the period before peak snow height and the period following peak snow height. While automatic measurements of snow water equivalent (SWE) were available from the SSG1000 snow scale (Sommer Messtechnik), we defined these periods based on snow height due to the uncertainty associated with the SWE measurements and to avoid potential bridging effects when ice crusts are present within the snowpack, which is a known limitation of the SSG1000 (Smith et al., 2017). The maximum SWE of 430 $\pm$ 43 mm w.e. (10% uncertainty) was measured on 12 April 2025, 12 days after peak snow height. During this period, manual snow measurements showed a substantial increase in bulk snowpack density from 309 kg m^{-3} on 3 April 2025 to 387 kg m^{-3} on 16 April 2025, coinciding with the formation of four ice crusts within the snowpack. The increase in snowpack density together with the decrease in snow height suggests ongoing snowpack compaction, while the formation of melt–refreeze crusts indicates internal melt–refreeze processes that may affect SWE measurements from the SSG1000.

Table 2 summarizes the mean meteorological conditions before and after peak snow height, and for full winter period. Mean wind speed remained relatively stable (2.15–2.23 m s^{-1}) across these periods. In contrast, both air temperature and snow surface temperature increased substantially after peak snow height, with mean air temperature rising from -4.7°C to 0.3 °C and snow surface temperature increasing from -9.6°C to -2.2°C. Net radiation showed a pronounced shift from negative daily mean values (-24 W m^{-2}) prior to peak snow height to positive daily mean values (19 W m^{-2}) following peak snow height, primarily driven by increased incoming shortwave radiation during in the later winter (Figure 3). The mean daily vapor pressure gradient also increased after peak snow height (from 50.5 to 57.4 Pa), reflecting larger difference between the saturation vapor pressure at the snow surface and the atmospheric vapor pressure at 5.4 m above the ground. Together, these changes show a shift towards

https://doi.org/10.5194/egusphere-2026-4268
Preprint. Discussion started: 5 August 2026

warmer and drier conditions after peak snow height, with increased energy availability through shortwave incoming radiation, and a drier atmosphere as shown by the higher vapor pressure gradient.

Table 2. Mean meteorological conditions before peak snow height (before peak HS; 19 November 2024 - 31 March 2025) and after peak snow height (after peak HS; 31 March 2025 - June 1 2025), and for the full winter period 2024-25 (19 November 2024 - June 1 2025) at the WFJ research site. The vapor pressure gradient is defined as the difference between saturation vapor pressure at the snow surface and actual vapor pressure at the measurement height (5.4 m above the ground).

	Before peak HS	After peak HS	Winter period
Wind speed (m s^{-1})	2.23	2.15	2.20
Air temperature (°C)	-4.7	0.4	-3.1
Snow surface temperature (°C)	-9.6	-2.2	-7.2
Net radiation (W m^{-2})	-24	19	-10
Saturation vapor pressure (Pa)	293.9	524.0	376.9
Vapor pressure (Pa)	243.4	466.6	315.2
Vapor pressure gradient (Pa)	50.5	57.4	52.7

4.2 Surface energy balance

Figure 3 shows the components of the surface energy balance as mean daily fluxes, with a summary for period before and after peak snow height shown in Table 3. Negative values indicate fluxes directed into the snowpack, and positive values represent fluxes directed away from the snowpack. A clear contrast in energy partitioning is observed between the two periods.

Before peak snow height, the energy balance was dominated by net longwave radiation emitted from the snowpack, with a mean daily contribution of 43 W m^{-2}, indicating radiative cooling of the snow surface. The latent heat flux (3.03 W m^{-2}) was relatively small but consistently positive (i.e., directed away from the snowpack), indicating that daytime sublimation exceeded nighttime deposition at the daily scale. Sensible heat flux (-12.31 W m^{-2}) and net shortwave radiation (-20 W m^{-2}), together with a small ground heat flux (-2.05 W m^{-2}), partially compensated for the snowpack energy losses, but were insufficient to offset the radiative deficit, resulting in a negative residual energy flux (-11 W m^{-2}). This residual term, which includes unmeasured components such as internal energy changes within the snowpack and any advected energy, was similar in magnitude to the sensible heat flux.

After peak snow height, the energy balance shifted markedly. Net shortwave radiation increased 3 times, reflecting larger incoming solar radiation. Net longwave radiation emitted from the snowpack showed negligible change. As a result, increasing net shortwave radiation dominated the energy balance, with net radiative inputs to the snowpack. Latent heat flux doubled (6.09 W m^{-2}) from before to after peak snow height (3.03 W m^{-2}), indicating higher sublimation rates, whereas sensible heat flux decreased by approximately 76%. The residual term became larger and positive (16 W m^{-2}), indicating warming of the snowpack.

https://doi.org/10.5194/egusphere-2026-4268
Preprint. Discussion started: 5 August 2026

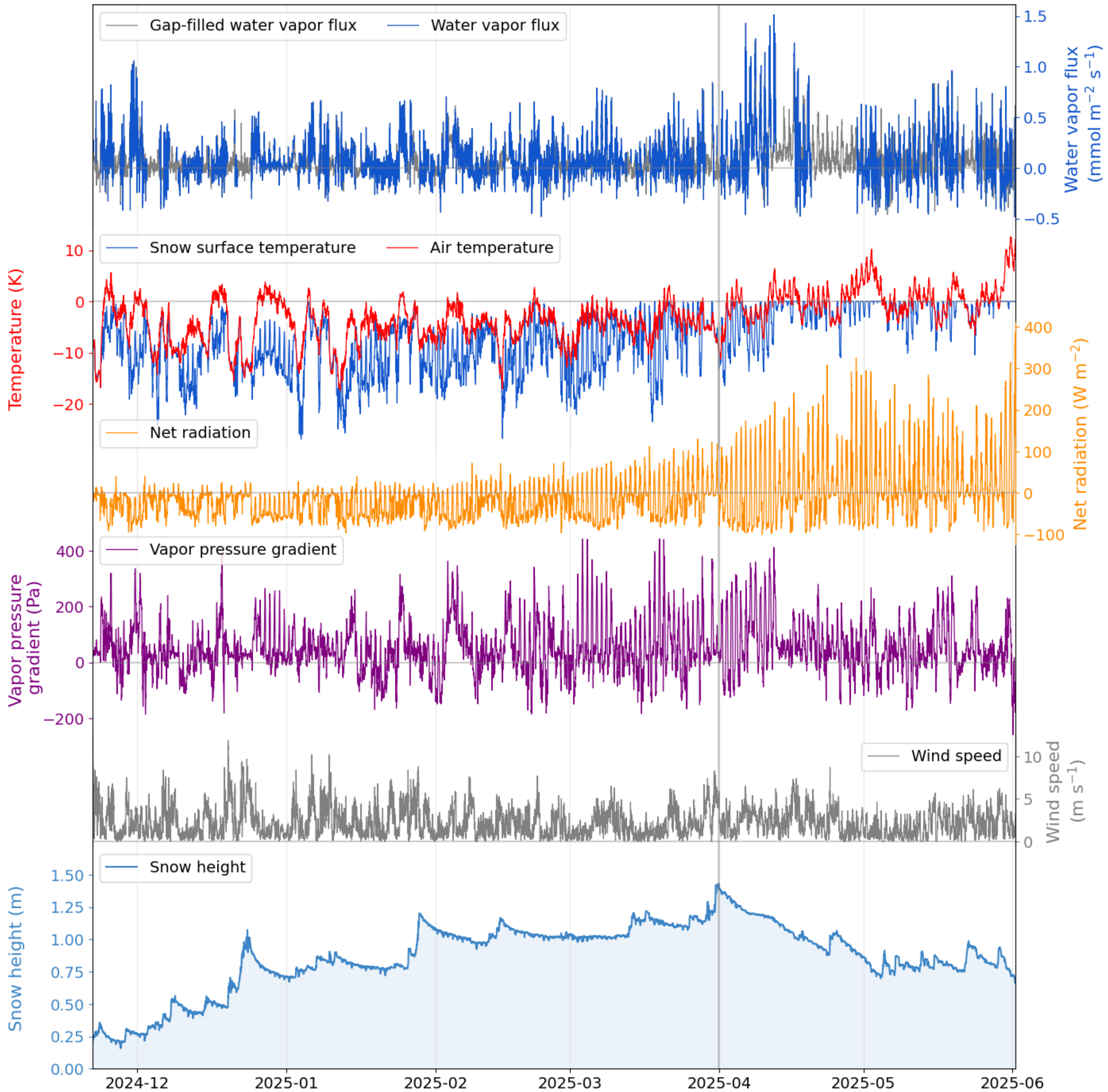

Figure 2. Overview of snowpack and meteorological conditions during the 2024-25 winter period at the WFJ research site. The displayed timeseries include measured and gap-filled water vapor fluxes, snow surface and air temperature, net radiation, vapor pressure gradient (defined as the difference between saturation vapor pressure at the snow surface and actual vapor pressure at 5.4 m above the ground), wind speed, and snow height. The timing of peak snow height is indicated by the vertical gray line, separating the winter into periods before and after peak snow height.

https://doi.org/10.5194/egusphere-2026-4268
Preprint. Discussion started: 5 August 2026

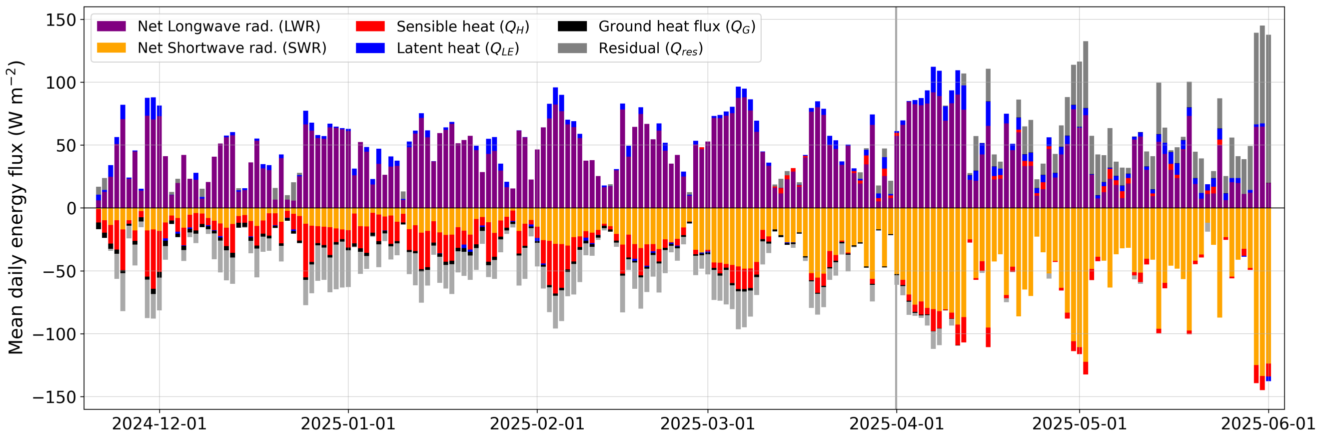

Figure 3. Mean daily snowpack energy budget terms for the winter period 2024-25. Components shown are net longwave radiation (LWR), net shortwave radiation (SWR), sensible heat flux (Q_H), latent heat flux (Q_{LE}), ground heat flux (Q_G) and a residual term (Q_{res}) as defined in Equation 6. Peak snow height is indicated with the gray vertical line. Note that fluxes entering the snowpack have a negative sign, while those exiting the snowpack have a positive sign.

Table 3. Average daily surface energy balance components before and after peak snow height (HS). All fluxes are given in W m^{-2}.

	Q_{LE}	Q_H	SWR	LWR	Q_G	Q_{res}
Before peak HS	3.03	−12.31	−20	43	-2.05	−11
After peak HS	6.09	−2.90	−62	43	0.03	16

The diurnal cycle of the different components of the snowpack energy balance, shown in Figure 4, provides more insights into differences before and after peak snow height. Incoming and outgoing longwave radiation exhibited weak diurnal variability during both periods (Figures 4a, 4b), with negligible seasonal change in net longwave radiation (Table 3), showing similar longwave radiation exchange between the snow surface and the atmosphere throughout the winter period. In contrast, net shortwave radiation showed a pronounced diurnal cycle, with substantially lower minima after peak snow height (approximately −620 W m^{-2}) compared to before peak snow height (approximately −420 W m^{-2}), indicating higher daytime radiative energy input after peak snow height.

Turbulent fluxes exhibited distinct seasonal and diurnal behavior (Figures 4c, 4d). Prior to peak snow height, latent heat flux remained close to zero during nighttime and exhibited peaks during daytime around noon, indicating sublimation fluxes during daytime. Following peak snow height, latent heat fluxes approximately doubled and exhibited a more sustained positive daytime flux, showing larger and prolonged sublimation. Sensible heat flux was consistently negative during nighttime prior to peak snow height, reflecting energy transfer from the atmosphere to the snowpack. During daytime, a weak positive peak flux was observed. In contrast, following peak snow height, the diurnal structure of sensible heat flux shifted to earlier in the day, with reduced nighttime fluxes and earlier daytime maximum values.

https://doi.org/10.5194/egusphere-2026-4268
Preprint. Discussion started: 5 August 2026

Table 4. Cumulative sublimation flux and average sublimation rate during the 2024-25 winter period, as well as before and after peak snow height (HS). Cumulative values include gap-filled fluxes. Hourly and daily rates are shown for non-gap-filled fluxes, with the estimated values after gap-filling shown in parentheses.

	Before peak HS	After peak HS	Winter period
Cumulative sublimation (mm)	12.6	12.1	24.7
Average hourly sublimation (mm h^{-1})	0.0053 (0.0040)	0.0097 (0.0082)	0.0065 (0.0054)
Average daily sublimation (mm d^{-1})	0.13 (0.097)	0.23 (0.20)	0.15 (0.12)

Prior to peak snow height, the residual energy flux exhibited minimal diurnal fluctuations and remained close to zero. However, after peak snow height, the residual fluxes showed pronounced diurnal cycles (Figures 4e, 4f), thereby becoming a major component of the diurnal energy budget, with negative nighttime values and daytime peaks exceeding 150 W m^{-2}. This indicates increased contributions from unmeasured processes after peak snow height, including (a) internal energy changes associated with melt–freeze activity in the snowpack, and (b) advected energy inputs.

Finally, during both periods, mean hourly air temperature remained higher than mean hourly snow surface temperature (Figures 4g, 4h). After peak snow height, average hourly snow surface temperature approached 0°C from 10:00 to 16:00, indicating an isothermal snowpack throughout most of the daytime.

4.3 Cumulative sublimation and sublimation rates

Cumulative net sublimation over the 2024-25 winter was 24.7 ± 18.3 mm (Figure 5), corresponding to 5.7 ± 4.2 % of the maximum snow water equivalent (SWE). The associated uncertainty of ± 18.3 mm was based on an assumed 20% systematic uncertainty for measured fluxes and the root mean squared error (RMSE) for gap-filled fluxes. This uncertainty represents a conservative upper-bound estimate of the total uncertainty.

Of the cumulative sublimation (24.7 mm) observed over the entire winter period, 12.6 mm occurred before peak snow height and 12.1 mm after peak snow height (Table 4). Although the two periods contributed almost equally to total sublimation, sublimation rates were substantially higher following peak snow height, even though it was shorter in duration (62 days vs 133 days). Mean hourly sublimation rate increased from 0.0053 mm h^{-1} prior to peak snow height to 0.0097 mm h^{-1} after peak snow height (Table 4). Similarly, the mean daily sublimation rate increased from 0.13 mm d^{-1} to 0.23 mm d^{-1} between these periods. The highest hourly sublimation rates were measured shortly after peak snow height, particularly in the first half of April (Figure 5), further highlighting the larger sublimation losses under late-winter and early-spring conditions.

Sublimation estimates based on gap-filled values were consistently lower than those derived from measured fluxes alone (Table 4), likely because missing observations mostly occurred during periods with overall small fluxes, such as during nighttime when stable atmospheric conditions occur. Nevertheless, the higher sublimation rates following peak snow height remained consistent across both measured and gap-filled datasets.

https://doi.org/10.5194/egusphere-2026-4268
Preprint. Discussion started: 5 August 2026

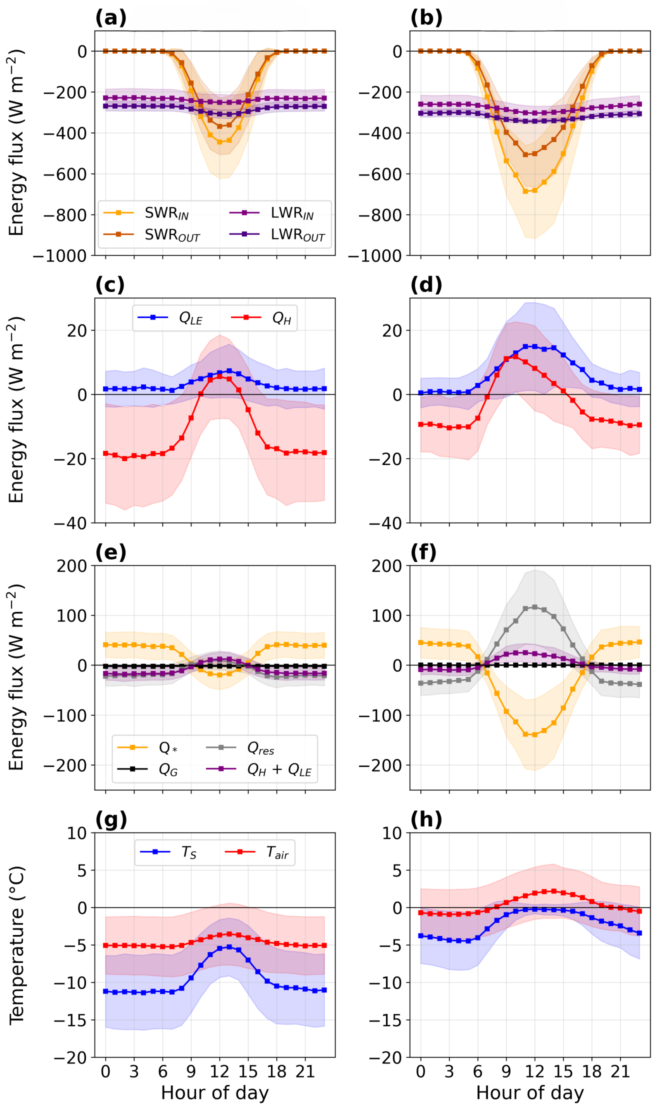

Figure 4. Diurnal cycle of mean hourly snowpack energy balance components. Left column shows values prior to peak snow height, and right column after peak snow height of winter 2024-25. Panels (a)–(b) show radiative fluxes, including incoming and outgoing shortwave and longwave radiation; panels (c)–(d) show turbulent fluxes of latent and sensible heat; panels (e)–(f) show the bulk energy balance terms; and panels (g)–(h) show air and snow surface temperature. Variables shown are incoming and outgoing shortwave radiation (SWR$_{IN}$, SWR$_{OUT}$), incoming and outgoing longwave radiation (LWR$_{IN}$, LWR$_{OUT}$), latent and sensible heat fluxes (Q$_{LE}$, Q$_H$), net radiation (Q$_*$), ground heat flux (Q$_G$), residual energy flux (Q$_{res}$), air temperature (T$_{air}$), and snow surface temperature (T$_S$). Fluxes directed toward the snowpack are negative, while fluxes directed away from the snowpack are positive.

https://doi.org/10.5194/egusphere-2026-4268
Preprint. Discussion started: 5 August 2026

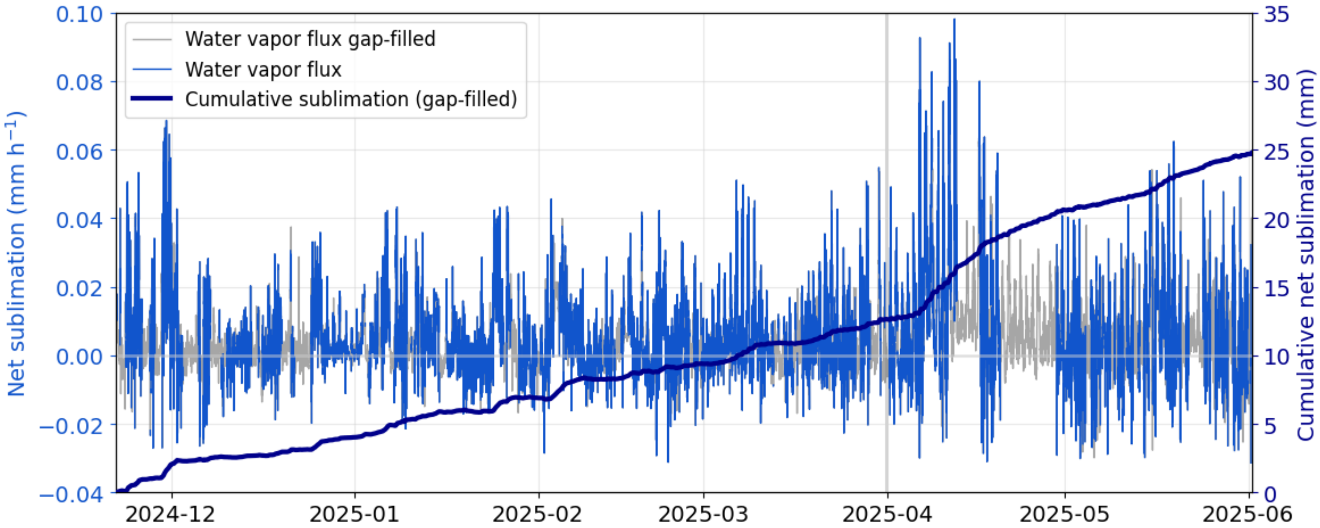

Figure 5. Temporal dynamics and evolution of net sublimation rates throughout the winter period 2024-25. Values are based on 15-minute aggregations of measured water vapor fluxes (blue) and gap-filled water vapor fluxes (light gray), with flux rates given in mm h^{-1}. Cumulative sublimation value, based on gap-filled water fluxes, throughout the winter period is shown in dark blue. The date of peak snow height is shown by gray vertical line.

4.4 Statistical drivers of sublimation

4.4.1 Correlations and partial correlations

Figure 6 presents the correlation matrix between net sublimation rate and the key meteorological drivers, using observations for the entire 2024-25 winter period (see Appendix A2 for the Pearson correlation matrix of all meteorological variables). All correlations in this section are statistically significant ($p < 0.01$), unless indicated otherwise. Net sublimation rate exhibited the strongest positive correlation with vapor pressure gradient (VPG; $r = 0.59$), net shortwave radiation (SWR; $r = 0.43$), net radiation ($r = 0.38$), and wind speed ($r = 0.34$). Relatively weaker correlations were seen with other drivers such as snow surface temperature ($r = 0.27$), relative humidity ($r = -0.26$), air temperature ($r = 0.21$), and net longwave radiation ($r = -0.17$). However, the meteorological variables were also strongly intercorrelated with each other, as shown in Figure 6. For example, snow surface temperature was strongly correlated with air temperature ($r = 0.68$), VPG with relative humidity ($r = -0.46$), and SWR with net radiation ($r = 0.87$). Only wind speed showed weak correlations with other meteorological variables ($r < 0.2$, all $p < 0.01$ except with SWR), suggesting a relatively independent atmospheric forcing.

To account for these strong cross correlations, we calculated the partial correlation coefficients between sublimation rate and relevant meteorological variables, to isolate the statistical association between sublimation and the individual meteorological drivers. Figure 7 presents partial correlation coefficients for the five key variables including VPG, wind speed, SWR, and snow

https://doi.org/10.5194/egusphere-2026-4268
Preprint. Discussion started: 5 August 2026

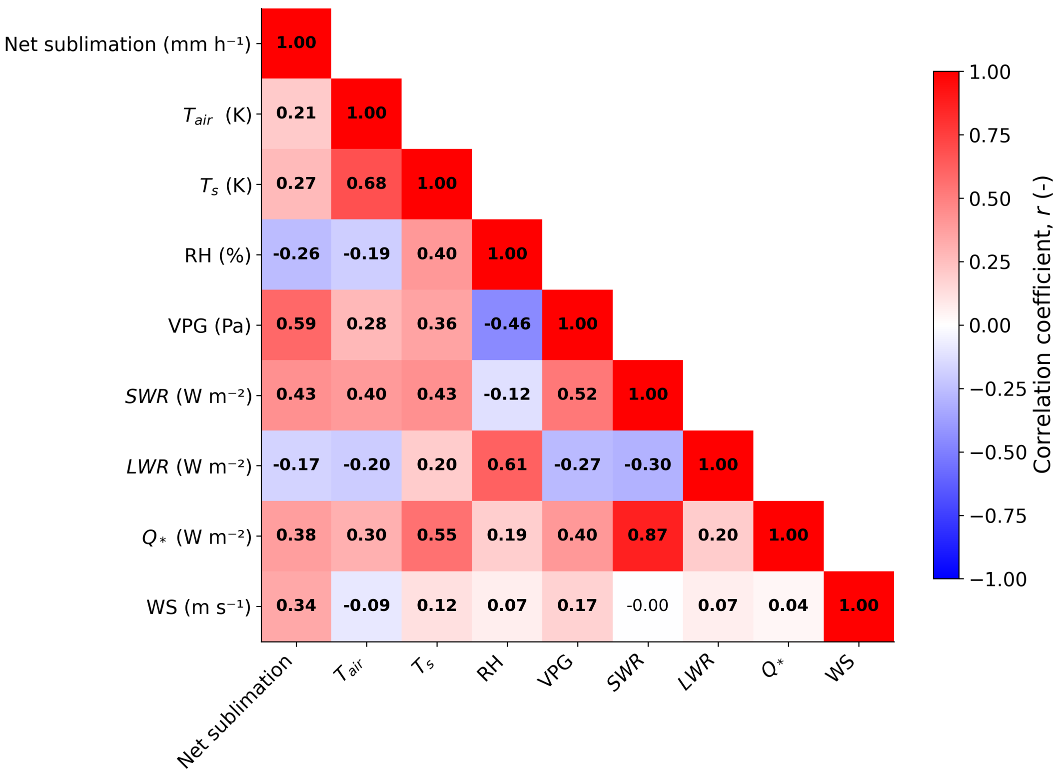

Figure 6. Pearson correlation coefficient (r) matrix for net sublimation rate and the driving meteorological variables for the winter period 2024-25: air temperature (T_A), snow surface temperature (T_S), relative humidity (RH), vapor pressure gradient (VPG), net shortwave radiation (SWR), net longwave radiation (LWR), net radiation (Q_*), and wind speed (WS). Statistically significant correlation values ($p < 0.01$) are indicated by bold fonts.

surface and air temperature using one, two, and three controlling variables. Net radiation was excluded because its correlation with sublimation became negligible after controlling for SWR ($r = -0.04$).

Partial correlation analysis revealed clear differences in the relative importance of meteorological controls on sublimation throughout the winter period (Figure 7a-e). VPG remained the dominant statistical driver of sublimation after controlling for three additional variables ($r = 0.44$), followed by wind speed ($r = 0.34$) and net shortwave radiation ($r = 0.23$). In contrast, air temperature and snow surface temperature showed weak to negative partial correlations ($r = -0.04$ and $r = -0.14$, respectively), indicating limited independent predictive power once covariance with other meteorological variables was accounted for.

VPG showed the strongest and most persistent relationship with sublimation rate, both from direct correlation and across partial correlations controlling for up to three variables. Although the correlation between VPG and sublimation decreased from $r = 0.59$ to $r = 0.44$ when accounting for three control variables, VPG consistently retained the highest partial correlation

https://doi.org/10.5194/egusphere-2026-4268
Preprint. Discussion started: 5 August 2026

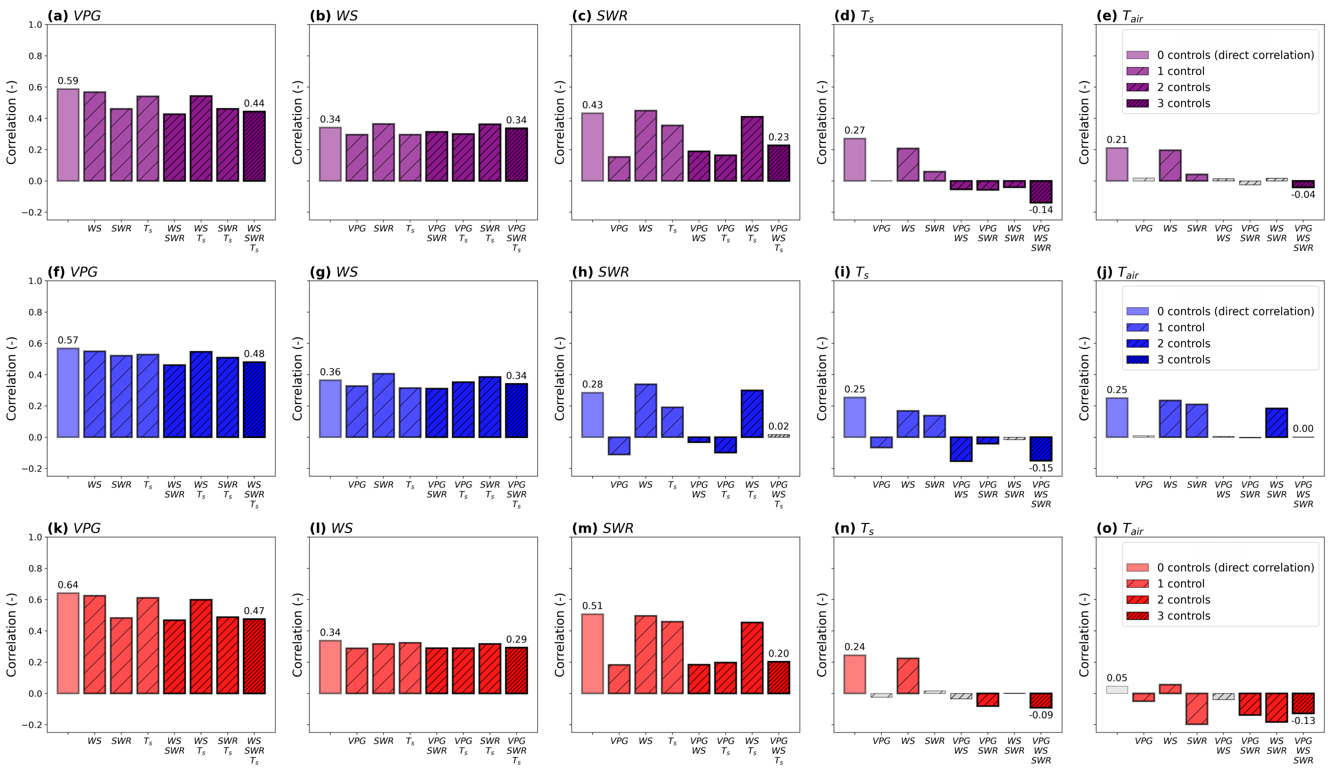

Figure 7. Correlations analysis for key driving variables. Shown are direct Pearson correlations and partial correlations for vapor pressure gradient (VPG), wind speed (WS), net shortwave radiation (SWR), snow surface temperature (T_S) and air temperature (T_A) with sublimation rate (mm h^{-1}) during the 2024-25 winter period (purple; top row), prior to peak snow height (blue; center row) and after peak snow height (red; bottom row). One, two and three controlling variables for partial correlations were applied, indicated by hatching of different width. The control variables used are indicated beneath the respective bar. Significant correlations ($p < 0.01$) are indicated by colored bars with bold outlines, while non-significant correlations are indicated by light gray bars.

among all variables. This pattern was evident both prior to (Figure 7f) and following peak snow height (Figure 7k), further highlighting VPG as the dominant statistical control on sublimation.

Wind speed showed a moderate but stable relationship with sublimation. Its partial correlation remained within a narrow range across all control configurations over the entire winter period ($r = 0.32$–0.37; Figure 7b). The partial correlation was slightly lower after peak snow height ($r = 0.29$), compared to before peak snow height ($r = 0.34$). Overall, differences in partial correlation values between these periods remained small, and wind speed emerged as the second most important statistical control on sublimation.

Net shortwave radiation exhibited a moderate direct correlation with sublimation rate ($r = 0.43$; Figure 7c) during the entire winter period, but this correlation substantially reduced to $r = 0.23$ when controlling for VPG, wind speed, and snow surface temperature. The reduction was pronounced before peak snow height, when the partial correlation after accounting for these

https://doi.org/10.5194/egusphere-2026-4268
Preprint. Discussion started: 5 August 2026

three controls was negligible and not statistically significant ($r = 0.02$, $p = 0.2$), whereas net shortwave radiation retained a significant independent association after peak snow height ($r = 0.20$, $p < 0.01$).

4.5 XGBoost and SHAP analysis

To complement the correlation-based analysis, we trained multiple XGBoost models to estimate sublimation rates from different combinations of meteorological variables. This approach allowed us to represent non-linear relationships between sublimation rates and its meteorological drivers. We then used SHAP values (Shapley Additive Explanations) to quantify the relative contribution of each meteorological variable and the interactions between different meteorological variables within the trained models.

Among the 21 tested model configurations using different combinations of meteorological forcings (Table A1), the highest predictive skill on the test dataset was achieved by models that included VPG, wind speed, radiation variables (SWR or net radiation), and snow surface temperature, with R^2 values of 0.56–0.58. Although training performance is also reported in Table A1, the interpretation below focuses on test dataset performance. Interestingly, all model configurations excluding VPG showed substantially lower predictive skill with $R^2 \leq 0.4$, supporting the partial correlation results that identified VPG as the dominant statistical control on sublimation. Notably, a model using only VPG and wind speed still achieved R^2 of 0.52, indicating that these two variables capture much of the explainable variability in sublimation rates and confirming their role as the primary meteorological controls on sublimation, consistent with Monin–Obukhov similarity theory.

Figure 8 shows the feature importance derived from the SHAP analysis for the selected XGBoost model, which included VPG, wind speed, SWR, and snow surface temperature as predictors. Feature importance was calculated as the mean absolute SHAP value for each variable (Wang et al., 2022), thereby quantifying the relative contribution of each feature to model prediction, with higher values indicating greater importance. Across all periods, VPG exhibited the highest feature importance, followed by wind speed, consistent with the partial correlation analysis. SWR and snow surface temperature had comparatively limited importance before peak snow height. After peak snow height, however, the importance of SWR increased substantially, reaching nearly three times the value before peak snow height. This indicates a stronger contribution of radiative forcing to sublimation late in the winter period and is consistent with the partial correlation results.

Figure 9 shows the temporal evolution of SHAP values throughout the winter period, together with the relationships between main and total SHAP values and their corresponding meteorological variables. SHAP values indicate how much each driver increases or decreases the baseline (mean) model prediction across the winter period, with positive values representing an increase and negative values representing a decrease relative to the baseline. VPG showed the largest SHAP values and exhibited a pronounced non-linear relationship with predicted sublimation (Figure 9b). Main SHAP values remained close to -0.01 mm h^{-1} for VPG values below approximately -25 Pa, corresponding to conditions in which atmospheric vapor pressure exceeded that of the snow surface and sublimation was suppressed. Above -25 Pa, main SHAP values increased almost linearly with VPG up to approximately 250 Pa. Beyond 250 Pa, main SHAP values plateaued near 0.02 mm h^{-1}, indicating limited additional increases in predicted sublimation under very strong vapor pressure gradients. The highest total SHAP values exceeded

https://doi.org/10.5194/egusphere-2026-4268
Preprint. Discussion started: 5 August 2026

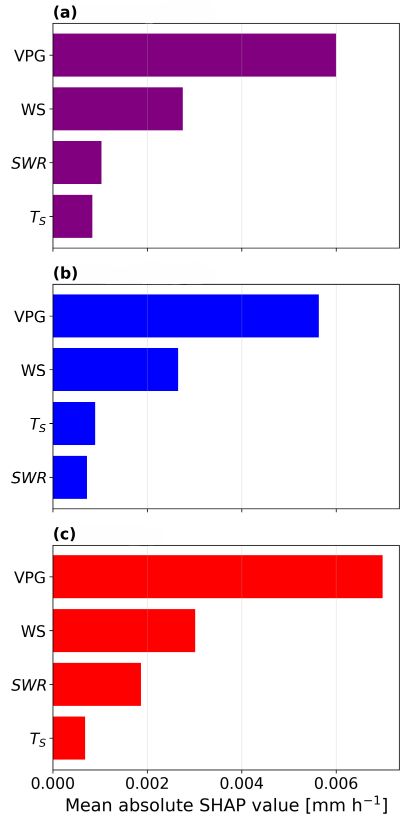

Figure 8. Global feature importance of vapor pressure gradient (VPG), wind speed (WS), net shortwave radiation (SWR), and snow surface temperature (T_S), calculated using the mean absolute SHAP values, for (a) the entire winter period, (b) before peak snow height, and (c) following peak snow height.

0.02 mm h^{-1} (Figure 9f), primarily due to interaction effect with SWR (Figure A4c) and, to a lesser extent, with wind speed (Figure A4a).

Wind speed showed a more linear relationship with SHAP values, with increasing wind speed consistently associated with higher SHAP values and therefore higher sublimation rates (Figure 9c and g). However, both main and total SHAP values for wind speed rarely exceeded 0.01 mm h^{-1}, indicating a weaker control on sublimation than VPG. SWR had relatively small main SHAP values across most of its range, remaining close to zero below approximately 200 W m^{-2} (Figure 9e). Above this threshold, the main SHAP values increased to between 0.005 and 0.008 mm h^{-1}, suggesting that higher radiative inputs increased sublimation. The highest total SHAP values approached 0.02 mm h^{-1}, largely reflecting interaction of SWR with VPG (Figure A3j). Snow surface temperature exhibited main and total SHAP values close to zero across its full range (Figure 9d and h), indicating a negligible independent contribution to modeled sublimation fluxes.

https://doi.org/10.5194/egusphere-2026-4268
Preprint. Discussion started: 5 August 2026

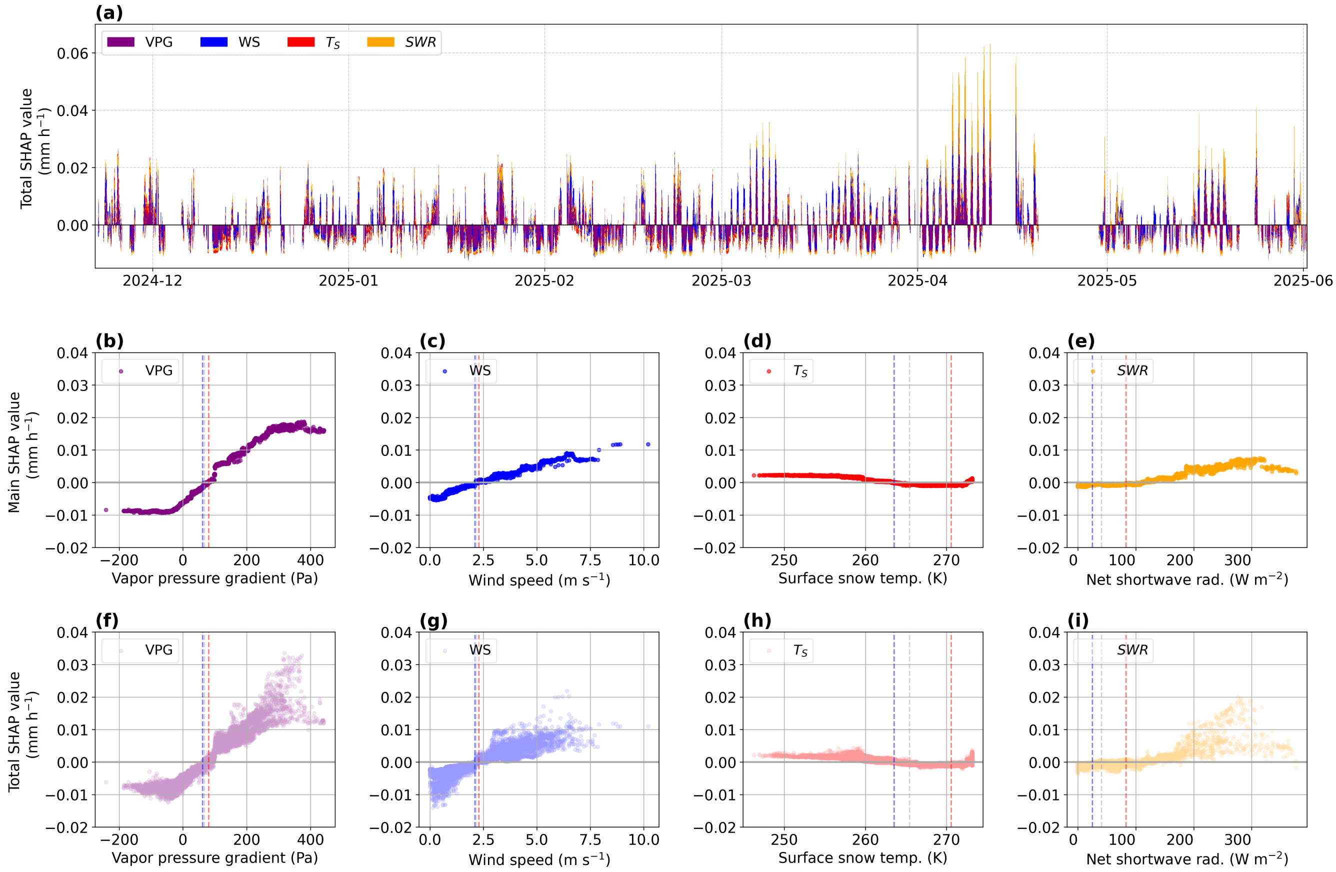

Figure 9. Temporal evolution of SHAP values throughout the 2024-25 winter period. (a) Feature contributions shown by total SHAP values including main and interaction effect – for vapor pressure gradient (VPG), wind speed (WS), snow surface temperature (Ts) and net shortwave radiation (SWR) on 15-minute water vapor fluxes. (b)-(e) Main SHAP values and (f)-(i) total SHAP values shown as a function of their respective predictor, with vertical blue and red lines showing the mean value of that predictor during before and after peak snow height.

5 Discussion

5.1 Magnitude and temporal dynamics of sublimation

Over the course of the winter period 2024-25, cumulative net sublimation at Weissfluhjoch was 24.7 ± 18.3 mm, corresponding to approximately 5% of maximum SWE, with an average daily flux of 0.15 $\mathrm{mm\,d^{-1}}$. This sublimation rate lies at the lower end of previous global compilations (Jackson and Prowse, 2009; Svoma, 2016; Mandal et al., 2022). Our sublimation estimate is most comparable to Reba et al. (2012), who reported cumulative net sublimation of 17 mm per winter over three seasons at a sheltered site in the Rocky Mountains, USA, equivalent to 0.15 $\mathrm{mm\,d^{-1}}$. It is also similar to Stockert et al. (2025), who reported cumulative sublimation of 21–24 mm (0.08-0.15 $\mathrm{mm\,d^{-1}}$) in seasonal snowpacks across tundra and boreal forest in

https://doi.org/10.5194/egusphere-2026-4268
Preprint. Discussion started: 5 August 2026

Alaska, USA, over 12 years. Higher cumulative sublimation of 32–34 mm, with mean rates of 0.26 $\mathrm{mm\,d^{-1}}$, was measured by Schwat et al. (2025) in a valley in the Rocky Mountains, USA, over a full winter season. Even higher winter sublimation rates of 0.32–0.52 $\mathrm{mm\,d^{-1}}$ have been reported at more wind-exposed sites in the Rocky Mountains, USA (Reba et al., 2012; Sexstone et al., 2016).

The relatively low sublimation flux observed at Weissfluhjoch can be explained by its local topography. The research site is sheltered by high surrounding ridges and experiences persistently low wind speeds (Figure1a, Table 2), which likely limits turbulent exchange and therefore reduces sublimation rates. In contrast, exposed alpine sites typically experience higher wind speeds and more frequent blowing-snow conditions, both of which can enhance turbulent exchange and increase sublimation losses (Schwat et al., 2025). Reba et al. (2012) reported substantially lower mean daily wind speeds at a sheltered site (1.2–1.4 m s^{-1}) than at a wind-exposed location (4.2–5.7 m s^{-1}), with lower sublimation rates at the sheltered site compared to the wind-exposed site (0.15 mm d^{-1} vs 0.32–0.52 mm d^{-1}). Similarly, previous modeling studies have indicated that surface sublimation in alpine terrain is highest at wind-exposed mountain ridges (Groot Zwaaftink et al., 2013).

Beyond these spatial controls, sublimation also exhibited strong temporal variability, with pronounced differences before and after peak snow height. Approximately half of the cumulative sublimation losses occurred before peak snow height, despite this period accounting for only one third of the snow cover duration. Average sublimation rates after peak snow height were nearly twice as high as before peak snow height (Section 4.3). Previous multiyear studies have also reported increasing sublimation rates toward the end of the winter season, with maximum rates typically occurring during the ablation period (Sexstone et al., 2016; Reba et al., 2012; Stockert et al., 2025). Likewise, Schwat et al. (2025) observed higher sublimation after the spring equinox, when net radiation became positive and SWE began to decline. Similarly, modeling studies have shown that snow-covered areas with greater energy availability tend to experience higher sublimation losses (Sprenger et al., 2024). Together, these findings suggest that the late winter period represents a disproportionately important phase for sublimation, despite its comparatively short duration.

The strong temporal variability in sublimation highlights the importance of measurement campaigns spanning full winter seasons to accurately capture seasonal dynamics and transitions between periods. At our site, for example, a short campaign conducted in early April would imply substantially higher seasonal sublimation rates than an equivalent campaign in early February (Figure 5). Short-duration measurement campaigns that are scaled to estimate seasonal totals may therefore introduce significant biases, depending on the timing of observations, because sublimation fluxes are highly episodic (Westermann et al., 2009; Svoma, 2016; Gustafson et al., 2010). Such sampling effects likely contribute to the wide range of sublimation estimates reported in the literature, particularly for studies based on limited seasonal coverage (Cullen et al., 2007).

5.2 Controls on sublimation

Based on the partial correlation and SHAP analyses, VPG and wind speed emerged as the dominant controls on sublimation, with VPG identified as the primary statistical control. This finding is consistent with previous studies that have highlighted the importance of atmospheric moisture gradients and wind speed in modulating sublimation.

https://doi.org/10.5194/egusphere-2026-4268
Preprint. Discussion started: 5 August 2026

Across glacier sublimation studies, multiple linear regression analyses have consistently revealed VPG and wind speed as the strongest predictors of sublimation (Mandal et al., 2022; Stigter et al., 2018). Similarly, in alpine terrain, Reba et al. (2012) found that VPG exhibited the strongest Pearson correlation with sublimation rates at both wind-sheltered and wind-exposed locations, while Stockert et al. (2025) reported the highest Pearson correlations between sublimation and atmospheric vapor pressure deficit across tundra and boreal forest landscapes. Both studies showed a consistent, but generally weaker, correlation between sublimation and wind speed ($r = 0.2$-0.64) (Stockert et al., 2025; Reba et al., 2012). These results are consistent with the physical mechanism of snow sublimation, in which the vapor pressure gradient between the snow surface and the overlying atmosphere governs the potential for water vapor transport away from the snowpack (Sexstone et al., 2016). Wind speed enhances turbulent mixing and helps maintain this vapor pressure gradient by removing moist air from the snow surface, thereby modulating sublimation rates (Lundquist et al., 2024).

The SHAP analysis further revealed a nonlinear response of sublimation to VPG, with the main SHAP values (representing sensitivity of sublimation rates to VPG when controlling for wind speed, snow surface temperature, and SWR) plateauing at VPG values of approximately 250 Pa. Above this threshold, higher total SHAP values (representing sublimation sensitivity to VPG while not controlling for other drivers) were achieved primarily through interactions with other variables, particularly wind speed and shortwave radiation. These interactions suggest that, while VPG provides the first-order potential for sublimation rates, additional meteorological conditions may be required to further enhance sublimation rates under high-VPG conditions (e.g., higher wind speeds can strengthen turbulent exchange and enhance sublimation). The apparent plateau in the VPG response may indicate a limitation in the mass-transfer rate under the conditions observed at Weissfluhjoch. However, this interpretation should be treated cautiously, as the VPG threshold may also reflect the XGBoost model behavior rather than a direct physical limit. Controlled experiments or additional observations across a wider range of meteorological conditions would be needed to confirm whether such a limitation of VPG on sublimation rates exists.

Both the SHAP and partial correlation analyses also showed that SWR became a more important control on sublimation after peak snow height. In the SHAP analysis, the SWR contribution became apparent above approximately 150 W m^{-2}. Previous studies have also reported correlations between net radiation and sublimation rates, with reported correlation values ranging from 0.36 to 0.60 (Stockert et al., 2025; Sexstone et al., 2016; Mandal et al., 2022). In addition, Schwat et al. (2025) qualitatively suggested a transition toward a radiation-driven regime of sublimation, based on observed increases in net radiation coinciding with enhanced sublimation. Together, these studies point to the statistical importance of radiative controls on sublimation, particularly in the late winter period.

However, the physical mechanism underlying this radiation effect remains unresolved. Enhanced radiation may increase liquid water content within the snowpack, allowing additional evaporation losses from the liquid water contained within the snow boundary layer (or evaposublimation). However, snowpack's liquid water content was not measured in this study. Another possibility is that shortwave radiation partly acts as a proxy for other unmeasured fluxes, such as advected heat flux, which may also influence sublimation rates (Schwat et al., 2026). Further research is required to disentangle these mechanisms, particularly because the highest sublimation rates occurred during this part of the season, as shown in Section 5.1.

https://doi.org/10.5194/egusphere-2026-4268
Preprint. Discussion started: 5 August 2026

In contrast to several previous studies, air temperature and snow surface temperature were not important independent statistical controls on sublimation at Weissfluhjoch. Previous studies in alpine and glaciated catchments have reported moderate correlations between temperature and sublimation rates, including air temperature and snow surface temperature correlations of 0.51 and 0.50, respectively, in Sexstone et al. (2016), air temperature correlations of 0.39 to 0.51 in Reba et al. (2012), and 0.62 to 0.69 in Mandal et al. (2022). In our analysis, however, Pearson correlations between sublimation rates and air temperature and snow surface temperature were smaller ($r = 0.27$ and $r = 0.21$, respectively). After controlling for VPG in the partial correlation analysis, air temperature exhibited negligible or even negative correlations with sublimation, indicating that temperature is not an independent control on sublimation at our site, but that its apparent influence was largely embedded within VPG. It is therefore the vapor pressure gradient that directly governs sublimation, consistent with Monin-Obukhov similarity theory. Similarly, higher snow surface temperatures independently have limited influence on sublimation, unless accompanied by a sufficient atmospheric moisture gradient to sustain vapor transport between the snowpack and the overlying atmosphere. This suggests that some previously reported temperature-sublimation relationships may partly reflect collinearity between temperature and VPG, rather than an independent control.

5.3 Uncertainties in estimated sublimation

The seasonal sublimation estimate of 24.7 mm at Weissfluhjoch includes a conservative seasonal uncertainty of ± 18.3 mm. This uncertainty combines a systematic uncertainty of 20% applied to measured turbulent fluxes, consistent with previous sublimation studies (Sexstone et al., 2016), as well as the uncertainty associated with gap-filled fluxes, estimated from the RMSE values of the gap-filling method. Due to instrument failure and periods that did not satisfy stationarity criteria, approximately 46% of turbulent flux measurements were missing and subsequently had to be gap filled using a random forest algorithm. Many of these missing periods occurred during weak-turbulence conditions, where turbulent fluxes are inherently difficult to resolve and the relative effect of gap-filling uncertainty on cumulative totals become proportionally larger. Reported uncertainties in previous sublimation studies in complex alpine terrain range from 12 to 50% (Sexstone et al., 2016; Schwat et al., 2025; Stiperski and Rotach, 2016), with the lower uncertainty of 12% derived from multi-height flux measurements (Schwat et al., 2025). However, several studies did not explicitly account for uncertainties associated with gap-filling (Schwat et al., 2025) or estimated seasonal sublimation by extrapolating short-term measurements (Reba et al., 2012). Importantly, the relatively large uncertainty primarily affects the cumulative seasonal sublimation estimates, whereas the reported hourly and daily sublimation rates, correlations, and SHAP analysis are based on non-gap-filled observations only.

Beyond the quantified uncertainty, sublimation fluxes at Weissfluhjoch may also be systematically underestimated. Previous EC measurements at 3 and 5m above the ground at Weissfluhjoch revealed negative vertical turbulent flux divergence, with turbulent fluxes measured at 3 m exceeding those measured at 5 m by approximately 10–25% (Stössel et al., 2010). The same study also reported a systematic underestimation of cumulative EC-derived sublimation relative to gravimetric surface mass loss measurements. Since our EC system was installed at approximately 5.4 m above the ground, similar flux divergence may have contributed to lower measured sublimation fluxes in this study, though this was not verified. Negative flux-divergence may occur due to stable or weakly stable atmospheric stratification above the snowpack, which suppresses buoyancy-driven turbulence

https://doi.org/10.5194/egusphere-2026-4268
Preprint. Discussion started: 5 August 2026

and limits vertical turbulent exchange (Lackner et al., 2022). At our site, snow surface temperatures remained persistently lower than air temperatures throughout much of the winter season (Figure 4g,h), indicating stable near-surface atmospheric conditions. In addition, the large residual energy term observed after peak snow height may indicate unmeasured energy contributions, including from melt-freeze processes, advected energy fluxes, or unresolved turbulent exchange. Advection and lateral turbulent fluxes may further contribute to snow–atmosphere exchange processes that are not fully captured by EC measurements (Schwat et al., 2025), while shallow boundary-layer development over snow may intermittently decouple the measurement height from the snow surface itself (Helgason and Pomeroy, 2012).

5.4 Climatological perspective

Finally, our findings need to be interpreted in the context of the 2024-25 winter period, which was a historically low snow year, with maximum SWE of 433 mm, which is 49% lower relative to the average maximum SWE of 849 mm between 1991-2020 (Haberkorn et al., 2025). Several multiyear studies have shown that surface sublimation rates show little variability between years and do not scale with snowpack SWE or depth (Sexstone et al., 2016; Reba et al., 2012). Therefore, sublimation has a larger effect on the overall water balance during dry winters with lower SWE (Sexstone et al., 2018; Drake et al., 2023). Years with similar snow cover duration, but contrasting SWE, may have comparable cumulative sublimation losses, but substantially different snowmelt volumes. As a result, dry winters, such as 2024-25, may lead to a larger proportion of winter snow accumulation lost as sublimation, thereby reducing the water available for melt and adversely affecting downstream water availability.

Snow cover duration has been declining at Weissfluhjoch and across the entire European Alps (Marty et al., 2025). During the 2024–25 winter, snow cover at Weissfluhjoch lasted from 11 November, 2024 to 14 June, 2025, marking the shortest record since 1936 and 39 days shorter compared to the 1999–2020 average (Haberkorn et al., 2025). This decrease of snow cover duration is particularly relevant given that the highest sublimation rates in our study occurred following peak snow height. Fewer snow-covered days in this period could therefore reduce the cumulative seasonal sublimation. However, it remains unclear whether shorter snow cover duration also reduces the relative importance of sublimation within the seasonal snow mass balance, particularly if sublimation rates remain high during late-winter and early-spring conditions. Resolving this requires multi-year observations spanning contrasting snow accumulation and snow cover regimes.

6 Conclusions

Eddy-covariance measurements at the Weissfluhjoch research site in the Eastern Swiss Alps during the 2024-25 winter season revealed cumulative net sublimation of 24.7 $\pm$ 18.3 mm, or 5.7 $\pm$ 4.2 % of maximum SWE, and an average sublimation rate of 0.15 mm d^{-1}. Nearly half (12.1 mm) of cumulative sublimation occurred after peak snow height, despite its substantially shorter duration, with mean sublimation rates increasing from 0.13 mm d^{-1} before peak snow height to 0.23 mm d^{-1} after peak snow height. This strong temporal variability highlights the importance of continuous winter-season measurements and shows that the late winter period disproportionately contributes to sublimation.

https://doi.org/10.5194/egusphere-2026-4268
Preprint. Discussion started: 5 August 2026

Partial correlation and SHAP analyses revealed vapor pressure gradient (VPG) as the dominant statistical control on sublimation, followed by wind speed. VPG exhibited the highest partial correlation and predictive power for estimating sublimation, confirming the primary role of the atmospheric moisture gradient in governing snow-atmosphere exchange. The SHAP analysis further indicated a non-linear VPG response, with main SHAP values plateauing at VPG values above 250 Pa. This suggests that, under high-VPG conditions, additional meteorological factors such as wind speed and shortwave radiation may be required to further enhance sublimation rates. Wind speed emerged as a robust and independent secondary statistical control on sublimation, with increasing wind speed consistently associated with higher sublimation.

Net shortwave radiation (SWR) emerged as a seasonally dependent statistical control on sublimation. Its contribution was negligible before peak snow height but increased substantially after peak snow height, particularly above approximately 150 W m^{-2}. This suggests that radiative forcing becomes more important during late-winter and early-spring conditions, when enhanced energy availability, melt-freeze processes, or advected energy fluxes may contribute to increased sublimation losses. In contrast, air temperature and snow surface temperature showed little independent predictive power once covariance with VPG was accounted for, indicating that their apparent influence on sublimation is largely embedded within the vapor pressure gradient.

Although the cumulative sublimation estimate is affected by substantial uncertainty, partly due to gap-filling and the challenges of resolving turbulent fluxes under weakly stable conditions, the results provide one of the first full winter-season estimates of surface snow sublimation in the European Alps using the eddy-covariance technique. The relatively low sublimation rates observed at Weissfluhjoch likely reflect the sheltered topographic setting and low wind speeds at the site. However, during low-snow winters such as 2024-25, even modest sublimation losses may represent a substantial fraction of the seasonal snow mass balance and reduce the subsequent water availability for spring melt. Multi-year eddy-covariance observations across contrasting climatic regimes are therefore needed to better constrain the role of sublimation in Alpine water budgets under climate warming.

Appendix A

Code and data availability. The code used for data processing and analyses, together with the processed 15-minute eddy-covariance fluxes and meteorological variables, are available through envidat.ch (URL to be provided upon publication). In-situ snow depth data from the Weissfluhjoch research site are freely available from https://www.slf.ch/en/services-and-products/slf-data-service.

Author contributions. IA: Conceptualization, Data curation, Formal analysis, Visualization, Methodology, Writing – Original Draft Preparation; RT: Supervision, Writing – Review and Editing; MF: Resources, Writing – Review and Editing; ML: Resources, Writing – Review and Editing, Funding Acquisition; HB: Conceptualization, Methodology, Supervision, Validation, Resources, Writing – Review and Editing

https://doi.org/10.5194/egusphere-2026-4268
Preprint. Discussion started: 5 August 2026

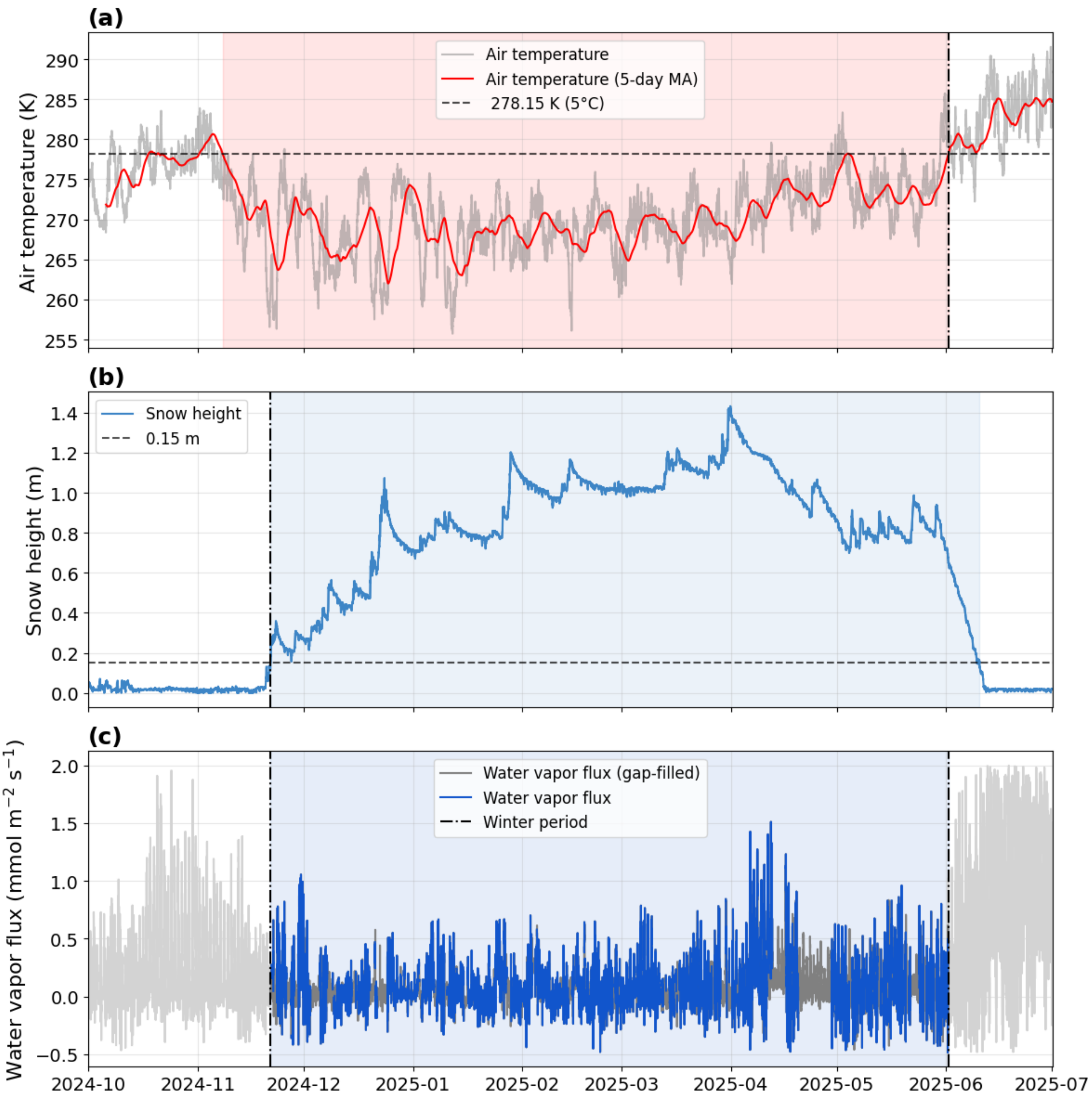

Figure A1. Rationale for choosing the specific winter period 2024-25 at the WFJ research site. (a) Air temperature (gray line) and the corresponding five day moving average (red). The threshold of 5°C for the moving average is shown by the dotted gray line and the corresponding time period when air temperature is below 5°C is shaded in pink. (b) Snow height in the winter period 2024-25 (blue) and the threshold of 15 cm (dashed gray line) indicating the time period in which continuous snow cover was there, without exposed rocks or bare soil (blue shading). (c) Raw (gray) and gap-filled (blue) water vapor fluxes, with the blue shading highlighting the selected winter period, which represents the overlap between the shaded areas in (a) and (b).

https://doi.org/10.5194/egusphere-2026-4268
Preprint. Discussion started: 5 August 2026

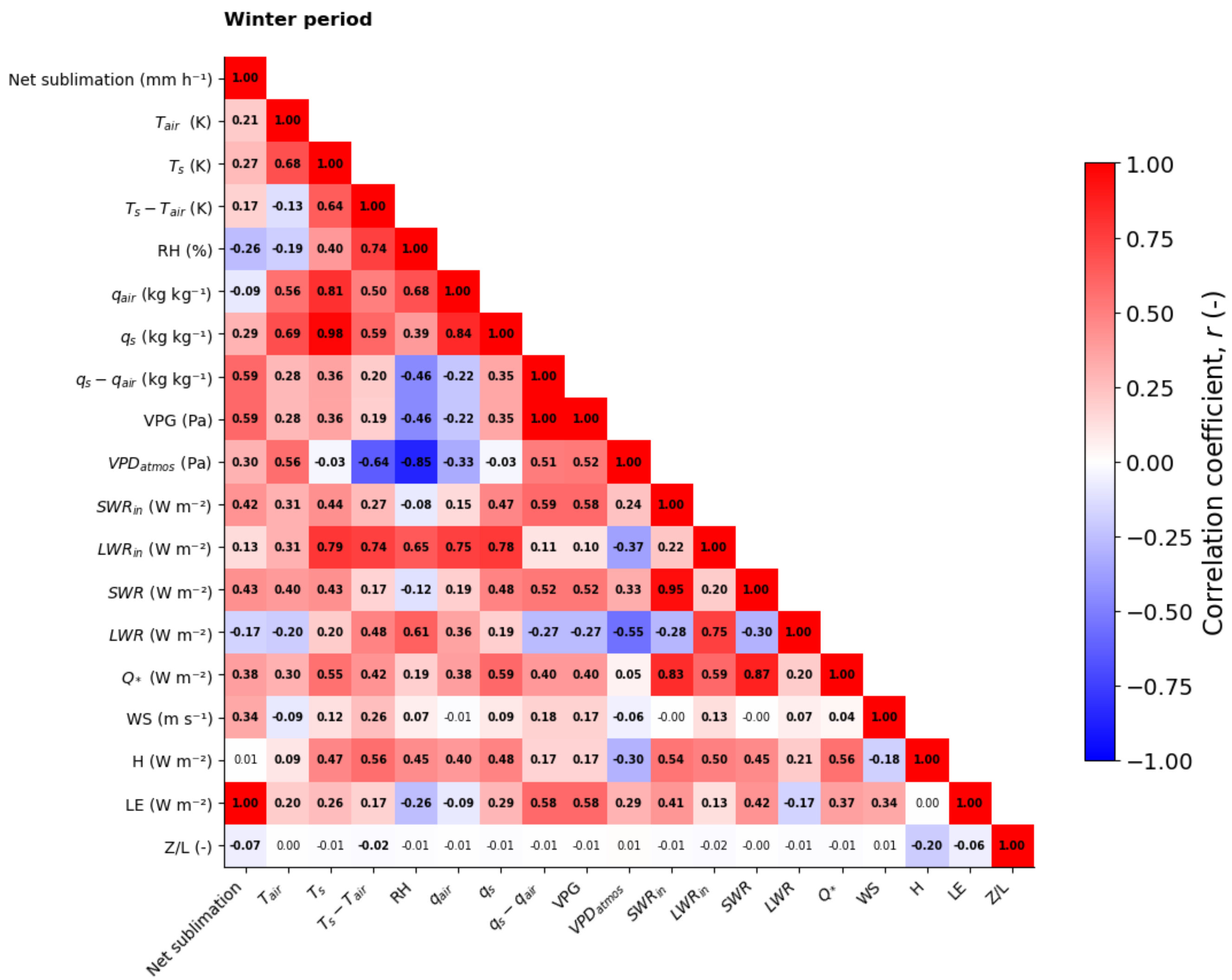

Figure A2. Extended Pearson correlation matrix of the following selected meteorological variables and sublimation rate throughout the winter period 2024-25: air temperature (T_{air}), snow surface temperature (T_S), relative humidity (RH), specific humidity in air (q_{air}) and snow (q_{snow}), vapor pressure gradient (VPG), atmospheric vapor pressure deficit (VPD_{atmos}), incoming shortwave radiation (SWR_{IN}), incoming longwave radiation (LWR_{IN}), net shortwave radiation (SWR), net longwave radiation (LWR), net radiation (Q_*), and wind speed (WS), sensible heat flux (H), latent heat flux (LE), stability parameter based on MOST (Z/L). Statistically significant correlations ($p < 0.01$) are indicated by bold values.

https://doi.org/10.5194/egusphere-2026-4268
Preprint. Discussion started: 5 August 2026

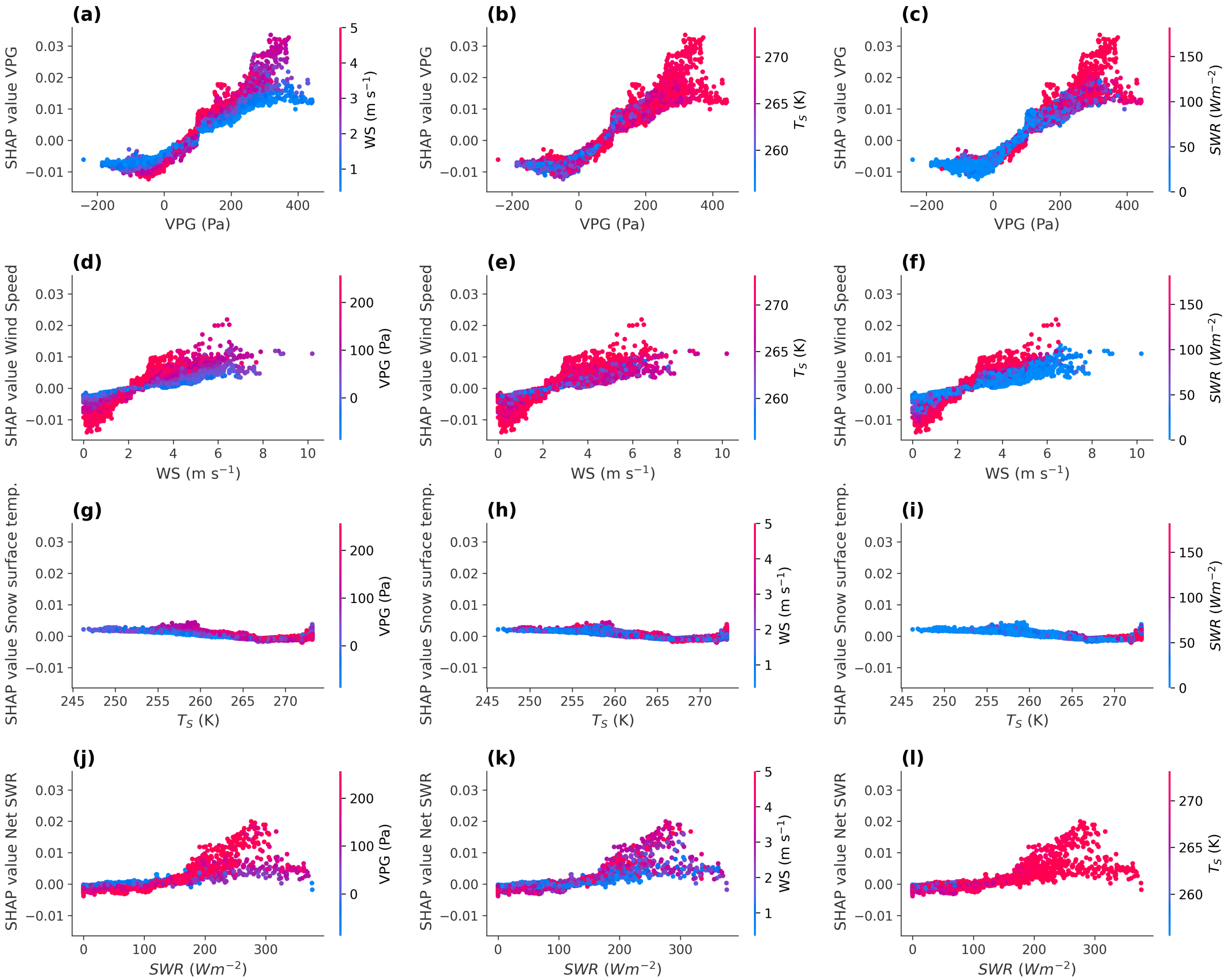

Figure A3. Dependency plots showing total SHAP values of a meteorological variable as a function of that variable, with the color bar indicating the value of another meteorological variable. Variables are vapor pressure gradient (VPG), wind speed (WS), snow surface temperature (T_S), and net shortwave radiation (SWR).

https://doi.org/10.5194/egusphere-2026-4268
Preprint. Discussion started: 5 August 2026

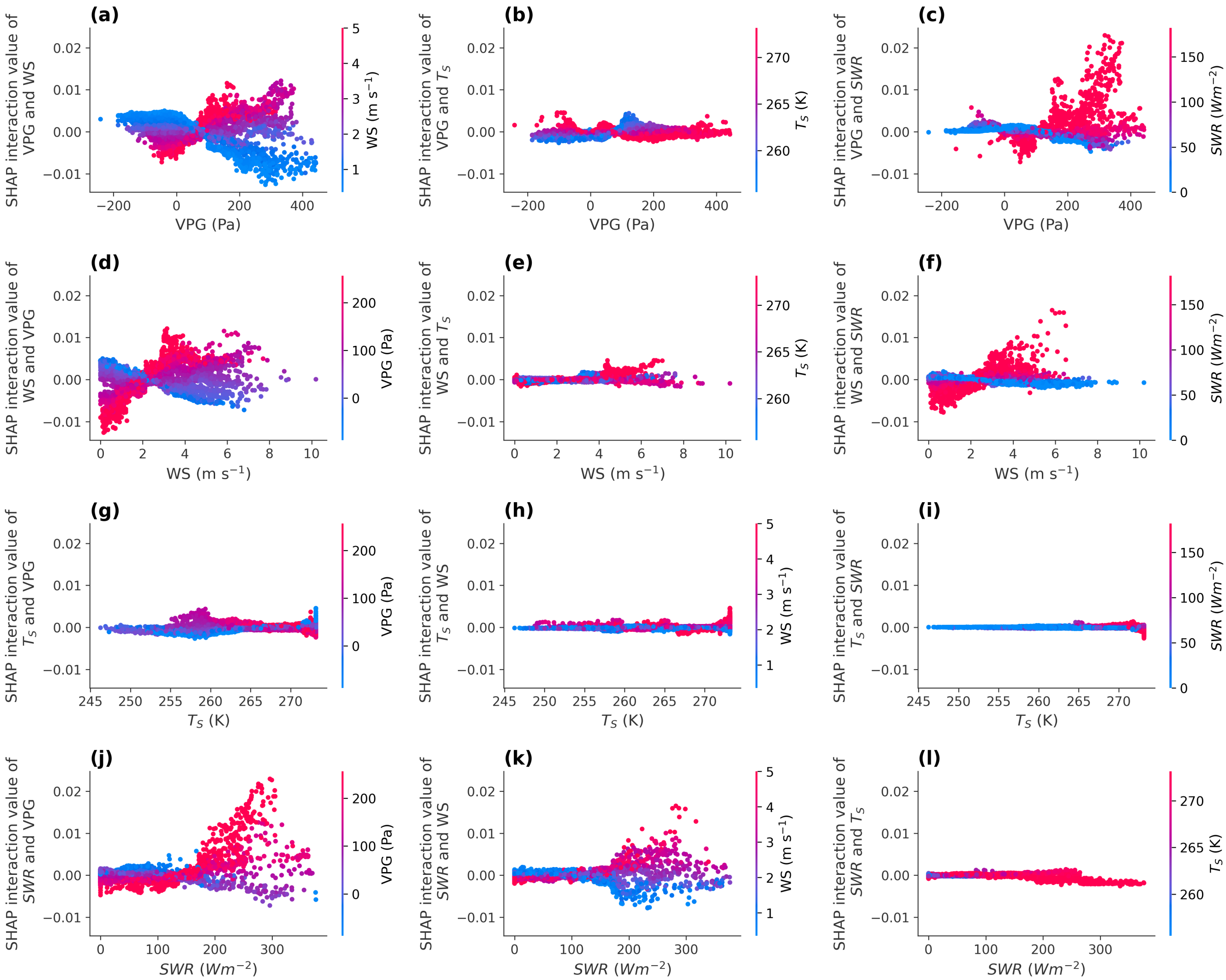

Figure A4. Interaction plots showing the interaction SHAP values of two meteorological variables, with the value of one variable shown on the x-axis and the other through the color bar. Variables are vapor pressure gradient (VPG), wind speed (WS), snow surface temperature (T_S), and net shortwave radiation (SWR).

https://doi.org/10.5194/egusphere-2026-4268
Preprint. Discussion started: 5 August 2026

Table A1. Performance of XGBoost models for different combinations of predictor variables. Variables are vapor pressure gradient (VPG), wind speed (WS), air temperature (T_{air}), snow surface temperature (T_S), net radiation (Q^*), and net shortwave radiation (SWR). Model performance is evaluated using mean squared error (MSE) and coefficient of determination (R^2) for training and test datasets.

Features	MSE Train	MSE Test	R^2 Train	R^2 Test
VPG, WS, T_S, Q^*	6.67×10^{-5}	7.55×10^{-5}	0.629	0.575
VPG, WS, T_S, SWR	7.46×10^{-5}	7.74×10^{-5}	0.586	0.564
VPG, WS, T_{air}, Q^*	5.86×10^{-5}	7.78×10^{-5}	0.674	0.562
VPG, WS, T_{air}, SWR	5.97×10^{-5}	7.88×10^{-5}	0.668	0.556
VPG, WS, Q^*	7.58×10^{-5}	7.90×10^{-5}	0.579	0.555
VPG, WS, SWR	7.68×10^{-5}	7.94×10^{-5}	0.573	0.553
VPG, WS, T_{air}	7.36×10^{-5}	8.05×10^{-5}	0.591	0.547
VPG, WS, T_S	7.87×10^{-5}	8.24×10^{-5}	0.563	0.536
VPG, WS	8.48×10^{-5}	8.58×10^{-5}	0.529	0.517
T_{air}, WS, SWR	1.04×10^{-4}	1.07×10^{-4}	0.424	0.400
T_{air}, WS, Q^*	8.53×10^{-5}	1.07×10^{-4}	0.526	0.397
T_S, WS, SWR	1.12×10^{-4}	1.09×10^{-4}	0.379	0.389
T_S, WS, Q^*	1.09×10^{-4}	1.11×10^{-4}	0.395	0.373
SWR, WS	1.16×10^{-4}	1.14×10^{-4}	0.353	0.357
Q^*, WS	1.16×10^{-4}	1.20×10^{-4}	0.355	0.322
SWR, T_{air}	1.29×10^{-4}	1.24×10^{-4}	0.282	0.302
SWR, T_S	1.34×10^{-4}	1.24×10^{-4}	0.255	0.299
Q^*, T_{air}	1.28×10^{-4}	1.30×10^{-4}	0.290	0.270
Q^*, T_S	1.35×10^{-4}	1.30×10^{-4}	0.252	0.267
T_S, WS	1.38×10^{-4}	1.40×10^{-4}	0.233	0.212
T_{air}, WS	1.40×10^{-4}	1.46×10^{-4}	0.221	0.176

565 *Acknowledgements.* HB and MF acknowledge the CryoSCOPE project (grant number: 101184736), funded by the State Secretariat for Education, Research and Innovation (SERI) under the European Union's Horizon Europe research and innovation program. We thank the WSL Institute for Snow and Avalanche Research SLF for maintaining the Weissfluhjoch research site and providing access to snow and meteorological observations.

References

Andreas, E. L., Persson, P. O. G., Jordan, R. E., Horst, T. W., Guest, P. S., Grachev, A. A., and Fairall, C. W.: Parameterizing Turbulent Exchange over Sea Ice in Winter, Journal of Hydrometeorology, 11, 87–104, https://doi.org/10.1175/2009JHM1102.1, 2010.

Barnett, T. P., Adam, J. C., and Lettenmaier, D. P.: Potential impacts of a warming climate on water availability in snow-dominated regions, Nature 2005 438:7066, 438, 303–309, https://doi.org/10.1038/nature04141, 2005.

Beria, H., Larsen, J. R., Ceperley, N. C., Michelon, A., Vennemann, T., and Schaefli, B.: Understanding snow hydrological processes through the lens of stable water isotopes, Wiley Interdisciplinary Reviews: Water, 5, 1–23, https://doi.org/10.1002/wat2.1311, 2018.

Chen, T. and Guestrin, C.: XGBoost: A scalable tree boosting system, Proceedings of the ACM SIGKDD International Conference on Knowledge Discovery and Data Mining, 13-17-August-2016, 785–794, 2016.

Cullen, N. J., Mölg, T., Kaser, G., Steffen, K., and Hardy, D. R.: Energy-balance model validation on the top of Kilimanjaro, Tanzania, using eddy covariance data, Annals of Glaciology, 46, 227–233, https://doi.org/10.3189/172756407782871224, 2007.

Drake, S. A., Nolin, A. W., and Oldroyd, H. J.: Near-field variability of evaposublimation in a montane conifer forest, Frontiers in Earth Science, Volume 11 - 2023, https://doi.org/10.3389/feart.2023.1249113, 2023.

Fierz, C., Armstrong, R. L., Durand, Y., Etchevers, P., Greene, E., McClung, D. M., Nishimura, K., Satyawali, P. K., and Sokratov, S. A.: The International Classification for Seasonal Snow on the Ground, Ihp technical documents in hydrology no. 83, iacs contribution no. 1, UNESCO-IHP, Paris, France, https://cryosphericsciences.org/publications/snow-classification/, last access: 18 May 2026, 2009.

Foken, T. and Wichura, B.: Tools for quality assessment of surface-based flux measurements, Agricultural and Forest Meteorology, 78, 83–105, https://doi.org/10.1016/0168-1923(95)02248-1, 1996.

Fratini, G., Ibrom, A., Arriga, N., Burba, G., and Papale, D.: Relative humidity effects on water vapour fluxes measured with closed-path eddy-covariance systems with short sampling lines, Agricultural and Forest Meteorology, 165, 53–63, https://doi.org/10.1016/j.agrformet.2012.05.018, 2012.

Groot Zwaaftink, C. D., Mott, R., and Lehning, M.: Seasonal simulation of drifting snow sublimation in Alpine terrain, Water Resour. Res, 49, 1581–1590, https://doi.org/10.1002/wrcr.20137, 2013.

Gustafson, J. R., Brooks, P. D., Molotch, N. P., and Veatch, W. C.: Estimating snow sublimation using natural chemical and isotopic tracers across a gradient of solar radiation, Water Resources Research, 46, https://doi.org/https://doi.org/10.1029/2009WR009060, 2010.

Haberkorn, A., Zweifel, B., Marty, C., and Techel, F.: Wetter, Schneedecke und Lawinengefahr in den Schweizer Alpen 2024/25, in: Schnee und Lawinen in den Schweizer Alpen, chap. 2, WSL-Institute fur Schnee und Lawinen Forschung, Davos, 2025.

Helgason, W. and Pomeroy, J.: Problems Closing the Energy Balance over a Homogeneous Snow Cover during Midwinter, Journal of Hydrometeorology, 13, 557–572, https://doi.org/10.1175/JHM-D-11-0135.1, 2012.

Howell, J. F. and Mahrt, L.: Multiresolution flux decomposition, Boundary-Layer Meteorology, 83, 117–137, https://doi.org/10.1023/A:1000210427798/METRICS, 1997.

Huss, M., Bookhagen, B., Huggel, C., Jacobsen, D., Bradley, R. S., Clague, J. J., Vuille, M., Buytaert, W., Cayan, D. R., Greenwood, G., Mark, B. G., Milner, A. M., Weingartner, R., and Winder, M.: Toward mountains without permanent snow and ice, Earth's Future, 5, 418–435, https://doi.org/10.1002/2016EF000514, 2017.

Hörtnagl, L.: QCF: overall quality control flag — CH-CHA Flux Product, 2025.

Hörtnagl, L.: diive: Python library for time series processing, https://doi.org/10.5281/zenodo.10884017, 2026.

https://doi.org/10.5194/egusphere-2026-4268
Preprint. Discussion started: 5 August 2026

Immerzeel, W. W., Lutz, A. F., Andrade, M., Bahl, A., Biemans, H., Bolch, T., Hyde, S., Brumby, S., Davies, B. J., Elmore, A. C., Emmer, A., Feng, M., Fernández, A., Haritashya, U., Kargel, J. S., Koppes, M., Kraaijenbrink, P. D., Kulkarni, A. V., Mayewski, P. A., Nepal, S., Pacheco, P., Painter, T. H., Pellicciotti, F., Rajaram, H., Rupper, S., Sinisalo, A., Shrestha, A. B., Viviroli, D., Wada, Y., Xiao, C., Yao, T., and Baillie, J. E.: Importance and vulnerability of the world's water towers, Nature 2019 577:7790, 577, 364–369, https://doi.org/10.1038/s41586-019-1822-y, 2019.

Jackson, S. I. and Prowse, T. D.: Spatial variation of snowmelt and sublimation in a high-elevation semi-desert basin of western Canada, 23, 2611–2627, https://doi.org/10.1002/hyp.7320, 2009.

Kljun, N., Calanca, P., Rotach, M. W., and Schmid, H. P.: A simple two-dimensional parameterisation for Flux Footprint Prediction (FFP), Geoscientific Model Development, 8, 3695–3713, https://doi.org/10.5194/GMD-8-3695-2015, 2015.

Knowles, J. F., Harpold, A. A., Cowie, R., Zeliff, M., Barnard, H. R., Burns, S. P., Blanken, P. D., Morse, J. F., and Williams, M. W.: The relative contributions of alpine and subalpine ecosystems to the water balance of a mountainous, headwater catchment, Hydrological Processes, 29, 4794–4808, https://doi.org/10.1002/HYP.10526, 2015.

Körner, C., Möhl, P., and Hiltbrunner, E.: Four ways to define the growing season, Ecology Letters, 26, 1277–1292, https://doi.org/https://doi.org/10.1111/ele.14260, 2023.

Lackner, G., Domine, F., Nadeau, D. F., Parent, A. C., Anctil, F., Lafaysse, M., and Dumont, M.: On the energy budget of a low-Arctic snowpack, Cryosphere, 16, 127–142, 2022.

Leibersperger, P., Asemann, P. L. E., and Engbers, R.: Processing Pipeline for Eddy Covariance Data Peddy.jl, https://doi.org/10.5281/zenodo.21235757, 2026.

LI-COR: EddyPro 7 | Calculating micrometeorological variables, 2025.

Lundberg, S. M., Erion, G., Chen, H., DeGrave, A., Prutkin, J. M., Nair, B., Katz, R., Himmelfarb, J., Bansal, N., and Lee, S. I.: From local explanations to global understanding with explainable AI for trees, Nature Machine Intelligence, 2, 56–67, https://doi.org/10.1038/S42256-019-0138-9;SUBJMETA, 2020.

Lundquist, J. D., Vano, J., Gutmann, E., Hogan, D., Schwat, E., Haugeneder, M., Mateo, E., Oncley, S., Roden, C., Osenga, E., and Carver, L.: Sublimation of Snow, Bulletin of the American Meteorological Society, 105, E975–E990, https://doi.org/10.1175/BAMS-D-23-0191.1, 2024.

Mandal, A., Angchuk, T., Azam, M. F., Ramanathan, A., Wagnon, P., Soheb, M., and Singh, C.: An 11-year record of wintertime snow-surface energy balance and sublimation at 4863ma.s.l. on the Chhota Shigri Glacier moraine (western Himalaya, India), Cryosphere, 16, 3775–3799, https://doi.org/10.5194/tc-16-3775-2022, 2022.

Marty, C.: Versuchsfeld Weissfluhjoch, https://www.slf.ch/de/ueber-das-slf/versuchsanlagen-und-labors/flaechen-und-anlagen-fuer-schnee-und-eis/versuchsfeld-weissfluhjoch/, 2025.

Marty, C. and Meister, R.: Long-term snow and weather observations at Weissfluhjoch and its relation to other high-altitude observatories in the Alps, Theoretical and Applied Climatology, 110, 573–583, 2012.

Marty, C., Michel, A., Jonas, T., Steijn, C., Muelchi, R., and Kotlarski, S.: SPASS – new gridded climatological snow datasets for Switzerland: potential and limitations, The Cryosphere, 19, 4391–4407, https://doi.org/10.5194/TC-19-4391-2025, 2025.

Mauder, M. and Foken, T.: UNIVERSITÄT BAYREUTH Documentation and Instruction Manual of the Eddy Covariance Software Package TK2, Arbeitsergebnisse Nr, 26, 1, 2004.

Meister, R.: Snow profiling at Weissfluhjoch, International Snow Science Workshop, 2009.

https://doi.org/10.5194/egusphere-2026-4268
Preprint. Discussion started: 5 August 2026

Moncrieff, J. B., Malhi, Y., and Leuning, R.: The propagation of errors in long-term measurements of land-atmosphere fluxes of carbon and water, Global Change Biology, 2, 231–240, https://doi.org/10.1111/J.1365-2486.1996.TB00075.X, 1996.

Montagnani, L., Grünwald, T., Kowalski, A., Mammarella, I., Merbold, L., Metzger, S., Sedlák, P., and Siebicke, L.: Estimating the storage term in eddy covariance measurements: the ICOS methodology, Int. Agrophys, 32, 551–567, https://doi.org/10.1515/intag-2017-0037, 2018.

Mott, R., Vionnet, V., and Grünewald, T.: The Seasonal Snow Cover Dynamics: Review on Wind-Driven Coupling Processes, Frontiers in Earth Science, Volume 6 - 2018, https://doi.org/10.3389/feart.2018.00197, 2018.

Poussin, C., Peduzzi, P., Chatenoux, B., and Giuliani, G.: A 37 years [1984–2021] Landsat/Sentinel-2 derived snow cover time-series for Switzerland, Scientific Data, 12, 632, https://doi.org/10.1038/s41597-025-04961-6, 2025.

Reba, M. L., Link, T. E., Marks, D., and Pomeroy, J.: An assessment of corrections for eddy covariance measured turbulent fluxes over snow in mountain environments, Water Resources Research, 45, 0–38, https://doi.org/10.1029/2008WR007045, 2009.

Reba, M. L., Pomeroy, J., Marks, D., and Link, T. E.: Estimating surface sublimation losses from snowpacks in a mountain catchment using eddy covariance and turbulent transfer calculations, Hydrological Processes, 26, 3699–3711, https://doi.org/10.1002/hyp.8372, 2012.

Rodell, M., Famiglietti, J. S., Wiese, D. N., Reager, J. T., Beaudoing, H. K., Landerer, F. W., and Lo, M.-H.: Emerging trends in global freshwater availability, https://doi.org/10.1038/s41586-018-0123-1, 2018.

Schwat, E., Hogan, D., Tha, K., Cox, C. J., Butterworth, B. J., Gutmann, E., Vano, J. A., and Lundquist, J. D.: Estimating Snow Sublimation in Complex Terrain: A Season of Intensive Field Measurements and the Role of Vertical Water Vapor Flux Divergence, https://doi.org/10.1175/JHM-D-25, 2025.

Schwat, E., Haugeneder, M., Reynolds, D., Hogan, D., Gutmann, E., and Lundquist, J. D.: Horizontal sensible heat advection increases snow melt rates: Beyond point measurements, EGUsphere, 2026, 1–30, https://doi.org/10.5194/egusphere-2026-1633, 2026.

Sexstone, G. A., Clow, D. W., Stannard, D. I., and Fassnacht, S. R.: Comparison of methods for quantifying surface sublimation over seasonally snow-covered terrain, Hydrological Processes, 30, 3373–3389, https://doi.org/10.1002/HYP.10864, 2016.

Sexstone, G. A., Clow, D. W., Fassnacht, S. R., Liston, G. E., Hiemstra, C. A., Knowles, J. F., and Penn, C. A.: Snow Sublimation in Mountain Environments and Its Sensitivity to Forest Disturbance and Climate Warming, Water Resources Research, 54, 1191–1211, https://doi.org/10.1002/2017WR021172, 2018.

Sigmund, A., Melo, D. B., Dujardin, J., Nishimura, K., and Lehning, M.: Parameterizing Snow Sublimation in Conditions of Drifting and Blowing Snow, Journal of Advances in Modeling Earth Systems, 17, e2024MS004 332, https://doi.org/https://doi.org/10.1029/2024MS004332, e2024MS004332 2024MS004332, 2025.

Smith, C. D., Kontu, A., Laffin, R., and Pomeroy, J. W.: An assessment of two automated snow water equivalent instruments during the WMO Solid Precipitation Intercomparison Experiment, The Cryosphere, 11, 101–116, https://doi.org/10.5194/tc-11-101-2017, 2017.

Sprenger, M., Carroll, R. W. H., Marchetti, D., Bern, C., Beria, H., Brown, W., Newman, A., Beutler, C., and Williams, K. H.: Stream water sourcing from high-elevation snowpack inferred from stable isotopes of water: a novel application of d-excess values, Hydrology and Earth System Sciences, 28, 1711–1723, https://doi.org/10.5194/hess-28-1711-2024, 2024.

Stigter, E. E., Litt, M., Steiner, J. F., Bonekamp, P. N., Shea, J. M., Bierkens, M. F., and Immerzeel, W. W.: The Importance of Snow Sublimation on a Himalayan Glacier, Frontiers in Earth Science, 6, https://doi.org/10.3389/feart.2018.00108, 2018.

Stiperski, I. and Rotach, M. W.: On the Measurement of Turbulence Over Complex Mountainous Terrain, Boundary-Layer Meteorology, 159, 97–121, https://doi.org/10.1007/s10546-015-0103-z, 2016.

https://doi.org/10.5194/egusphere-2026-4268
Preprint. Discussion started: 5 August 2026

Stockert, K. A., Euskirchen, E. S., and Stuefer, S. L.: Sublimation measurements of tundra and taiga snowpack in Alaska, The Cryosphere, 19, 1739–1755, https://doi.org/10.5194/tc-19-1739-2025, 2025.

Stössel, F., Guala, M., Fierz, C., Manes, C., and Lehning, M.: Micrometeorological and morphological observations of surface hoar dynamics on a mountain snow cover, Water Resources Research, 46, https://doi.org/10.1029/2009WR008198, 2010.

Strasser, U., Bernhardt, M., Weber, M., Liston, G. E., and Mauser, W.: The Cryosphere Is snow sublimation important in the alpine water balance?, Tech. rep., www.the-cryosphere.net/2/53/2008/, 2008.

Svoma, B. M.: Difficulties in Determining Snowpack Sublimation in Complex Terrain at the Macroscale, Advances in Meteorology, 2016, 1–10, https://doi.org/10.1155/2016/9695757, 2016.

Vickers, D. and Mahrt, L.: Quality Control and Flux Sampling Problems for Tower and Aircraft Data, Journal of Atmospheric and Oceanic Technology, 14, 512–526, https://doi.org/10.1175/1520-0426(1997)014<0512:QCAFSP>2.0.CO;2, 1997.

Vickers, D. and Mahrt, L.: The Cospectral Gap and Turbulent Flux Calculations, Tech. rep., 2003.

Wang, H., Yan, S., Ciais, P., Wigneron, J. P., Liu, L., Li, Y., Fu, Z., Ma, H., Liang, Z., Wei, F., Wang, Y., and Li, S.: Exploring complex water stress–gross primary production relationships: Impact of climatic drivers, main effects, and interactive effects, Global Change Biology, 28, 4110–4123, https://doi.org/10.1111/gcb.16201, 2022.

Webb, E. K., Pearman, G. I., and Leuning, R.: Correction of flux measurements for density effects due to heat and water vapour transfer, Quarterly Journal of the Royal Meteorological Society, 106, 85–100, https://doi.org/10.1002/QJ.49710644707, 1980.

Westermann, S., Lüers, J., Langer, M., Piel, K., and Boike, J.: The annual surface energy budget of a high-arctic permafrost site on Svalbard, Norway, The Cryosphere, 3, 245–263, https://doi.org/10.5194/tc-3-245-2009, 2009.

Wilczak, J. M., Oncley, S. P., and Stage, S. A.: Sonic anemometer tilt correction algorithms, Boundary-Layer Meteorology, 99, 127–150, https://doi.org/10.1023/A:1018966204465/METRICS, 2001.